



Late Weichselian and Holocene behavior of the Greenland Ice Sheet in the Keiser Franz Josef Fjord system, NE Greenland[☆]



Ingrid Leirvik Olsen^{a,*,1}, Jan Sverre Laberg^a, Matthias Forwick^a, Tom Arne Rydningen^a, Katrine Husum^b

^a Department of Geosciences, UiT the Arctic University of Norway, Post Box 6050 Langnes, 9037, Tromsø, Norway

^b Norwegian Polar Institute, Post Box 6606 Langnes, 9296, Tromsø, Norway

ARTICLE INFO

Article history:

Received 6 December 2021

Received in revised form

31 March 2022

Accepted 1 April 2022

Available online xxx

Handling Editor: Dr C. O'Cofigaigh

Keywords:

Greenland Ice sheet

NE Greenland

Late weichselian

Holocene

Submarine landforms

Marine sediment cores

Ice stream retreat dynamics

Paleoenvironment

ABSTRACT

To better understand the past retreat patterns and chronologies of major marine-terminating outlet glaciers, the Late Weichselian and Holocene glacial history of a NE Greenland fjord system is reconstructed using new and previously published swath bathymetry and high-resolution seismic data, supplemented with multi-proxy analysis of sediment cores. The investigated area extends more than 190 km, including Fosters Bugt, Keiser Franz Josef Fjord, Nordfjord and Moskusoksefjord, the drainage routes for Waltershausen Gletscher, one of the largest outlet glaciers in the NE sector of the Greenland Ice Sheet. A complex of moraine ridges identified in Fosters Bugt show former stillstand positions during this period, and, alongside radiocarbon ages, supports the theory of a maximum ice front position in the outer coastal areas during the Younger Dryas-Preboreal period. The retreat moraines distributed within the Keiser Franz Josef Fjord system provide evidence of a stepwise retreat during the last deglaciation, whereby rapid retreat was interrupted by episodes of stillstands and/or readvances of the grounding line. The fjord system was mostly deglaciated prior to 7.8 ka cal BP, with an estimated average retreat rate ranging between 33 and 96 m a⁻¹ since the Younger Dryas. Following this, only minor ice advances in the inner fjords have been identified. The sediment supply from Waltershausen Gletscher dominated the Keiser Franz Josef Fjord, Nordfjord and outer Moskusoksefjord throughout the Holocene period, whereas in the middle and inner Moskusoksefjord the sediment deposits reflect a more local catchment area. The estimated average retreat rate is in the same order of magnitude as the rates from fjords of northern Fennoscandia, indicating the same overall control for the deglaciation, ice melting from increased Northern Hemisphere summer insolation that peaked in Early Holocene.

© 2022 The Authors. Published by Elsevier Ltd. This is an open access article under the CC BY license (<http://creativecommons.org/licenses/by/4.0/>).

1. Introduction

Marine-terminating outlet glaciers play an important role in controlling the mass balance of the Greenland Ice Sheet (GrIS), and

around 280 outlet glaciers presently terminate in fjords, discharging a total of ~500 Gt of ice annually (Catania et al., 2019; Mankoff et al., 2019). Many marine-terminating glaciers are now accelerating, thus, potentially contributing to a substantial sea-level rise (Pritchard et al., 2009). This increase in mass loss from the GrIS has resulted in a negative mass balance, contributing 2.7 mm sea level rise per year over the two last decades (Muntjewerf et al., 2020). However, on a longer time scale, i.e. from the last glacial and up to present, little is still known about the behavior of these outlet glaciers. A better understanding of the retreat patterns and chronologies of major marine-terminating outlet glaciers in Greenland is needed to more precisely predict their sensitivity and future behavior to external forcing. Fjord archives, including fjord bathymetry and sediment records, can help to improve our understanding of how outlet glaciers drained the GrIS in the past, as fjords act as efficient sediment traps and are relatively sensitive to

[☆] The idea of the study developed from repeated discussions among the authors of this study and the opportunity to participate in multiple scientific cruises to the study area. JS, MF and KH collected the new data during the TUNU V cruise. The geophysical and lithological data were interpreted by ILO in collaboration with MF, JSL and TAR. ILO conducted sample preparation and analyses of sediment data with help from JSL and KH. ILO wrote the manuscript with contributions from all authors.

* Corresponding author.

E-mail address: Ingrid.leirvik.olsen@ngu.no (I.L. Olsen).

¹ Present address: Geological Survey of Norway (NGU), Post Box 6315, Torgården, 7491, Trondheim, Norway.

environmental changes (Howe et al., 2010).

Multiple studies on the glaciation history have been performed in fjords on NW Greenland (e.g. Batchelor et al., 2018; Jakobsson et al., 2018; Hogan et al., 2020) and SE Greenland (e.g. Andrews et al., 1994; Jennings and Weiner, 1996; Dyke et al., 2014; Batchelor et al., 2019; Vermassen et al., 2020). Comparable studies from NE Greenland fjords are sparse, and limited to Scoresby Sund (e.g. Marienfeld, 1992; Dowdeswell et al., 1994; Ó Cofaigh et al., 2001), Keiser Franz Josef Fjord (Evans et al., 2002), Young Sund-Tyrolerfjord (e.g. Kroon et al., 2017; Ribeiro et al., 2017; Luostarinen et al., 2020) and offshore 79° N Glacier (e.g. Lindeman et al., 2020; An et al., 2021). Evans et al. (2002) presented the, thus far, most extensive geophysical/geological study of a fjord system on NE Greenland north of Scoresby Sund. Analysis of sub-bottom profiler data and sediment cores in Keiser Franz Josef Fjord (Fig. 1) showed that the fjord was filled with a grounded ice stream during the Last Glacial Maximum (LGM), while the reconstructions of the deglacial dynamics and timing of the glacier retreat in the region also include analyses of marine and terrestrial landforms as well as lake (e.g. Hjort, 1979; Wagner et al., 2000, 2010; Evans et al., 2002; Wagner and Melles, 2002; Arndt, 2018).

We here integrate new swath bathymetry, high-resolution seismic data and multi-proxy analysis of sediment cores in a 190 km long transect extending from the NE Greenland outer coastline to inner Moskusoksefjord. This area is within the drainage route for Waltershausen Gletscher, one of the largest outlet glaciers in the NE sector of the GrIS, and includes Fosters Bugt, Keiser Franz Josef Fjord, Nordfjord and Moskusoksefjord (Fig. 1). The results include submarine landform assemblages, sedimentary facies, sedimentation rates, seismic facies and observations of onshore

landforms. From this we reconstruct sedimentary processes and the paleoenvironmental development of the area, including also an updated (recalibrated) deglacial chronology, all of which improve the understanding of the Late Weichselian and Holocene behavior of this part of the GrIS.

2. Background

2.1. Physiographic setting

Keiser Franz Josef Fjord is a branched fjord system located on the northeastern coast of Greenland between $\sim 73^{\circ}00'$ and $74^{\circ}00'$ N that opens towards Fosters Bugt and the Greenland Sea (Fig. 1). The fjord system is ~ 220 km long, covers an area of 2200 km² (Evans et al., 2002) and includes the trunk fjord Keiser Franz Josef Fjord, as well as the tributary fjords Isfjord, Geologifjord, Nordfjord and Moskusoksefjord. The GrIS presently drains into the Keiser Franz Josef Fjord system via the marine terminating glaciers Waltershausen-, Adolf Hoel-, Jætte-, Gerrard de Geer- and Nordenskjöld Gletschers (Fig. 1b).

The inner and outer parts of the Keiser Franz Josef Fjord system (the actual Keiser Franz Josef Fjord) are NW-SE oriented, 10–20 km wide and up to 550 m deep. The transition to Nordfjord is defined by a marked sill (Fig. 1c), see also Evans et al. (2002). Nordfjord and Moskusoksefjord constitute the northern elongation of the Keiser Franz Josef Fjord system; they are separated by Gauss Halvø peninsula (Fig. 1b). Nordfjord is 35 km long and 13 km wide, and its orientation changes from SE-NW to S-N towards the terminus of Waltershausen Gletscher. Moskusoksefjord is ~ 65 km long and 0.6–5 km wide. Moskusoksefjord continues on land as a valley,

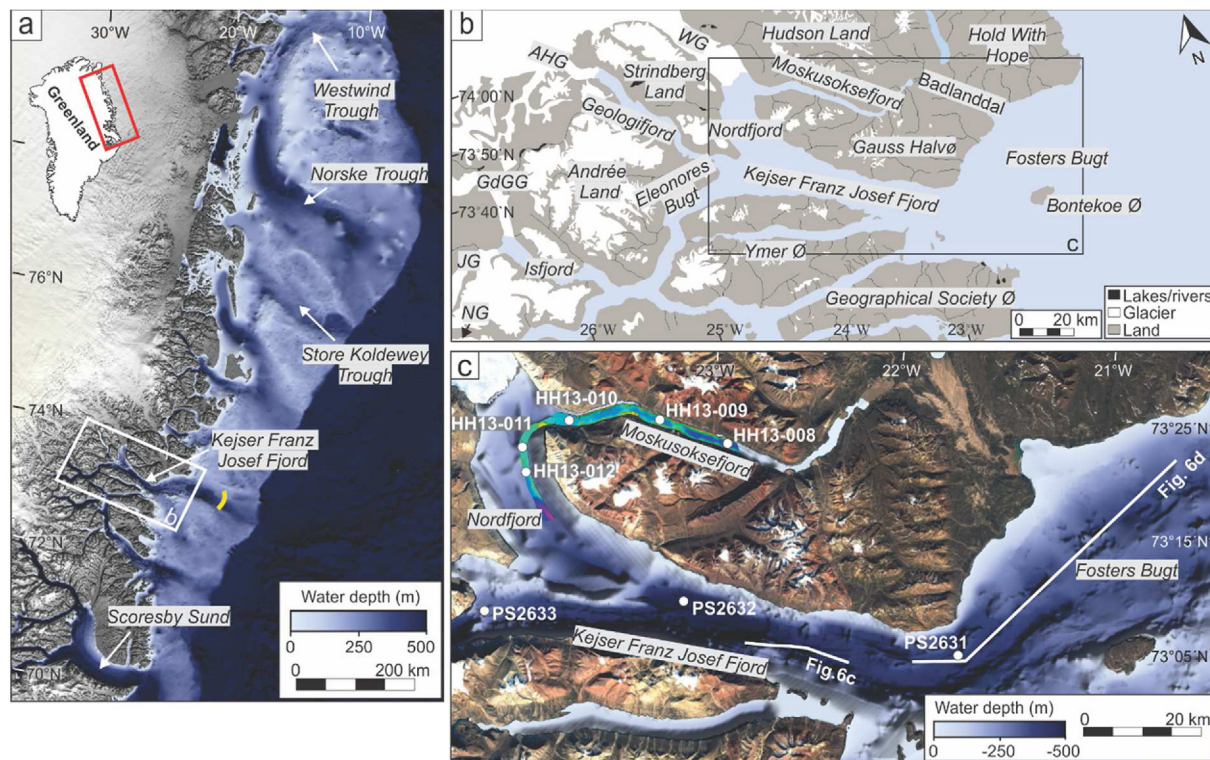


Fig. 1. (a) Overview map of NE Greenland, showing the large-scale bathymetry of the fjords and continental shelf (from IBCAO v. 4.0; Jakobsson et al. (2020)). The location of the study area (b) and geographical place names are indicated. Yellow line show the location of a mapped mid-shelf grounding zone wedge off the coast of Keiser Franz Josef Fjord (Evans et al., 2002; Arndt, 2018). (b) Overview map of the study area. Glaciers and major river systems are indicated. WG = Waltershausen Gletscher, AHG = Adolf Hoel Gletscher, GdGG = Gerrard de Geer Gletscher, JG = Jætte Gletscher, NG = Nordenskjöld Gletscher. (c) Large-scale bathymetry of the study area (from IBCAO v. 4.0; Jakobsson et al. (2020)), including the locations of the sediment cores and swath bathymetry analyzed in this study. Background topography image from Copernicus Sentinel Data (2020). (For interpretation of the references to color in this figure legend, the reader is referred to the Web version of this article.)

Badlanddal, which can be followed to the sea in a bay ~30 km north of the Kejsler Franz Josef Fjord entrance. The orientation of the fjord axis varies, but the overall orientation is E-W.

The width of the calving front of the tidewater glacier Waltershausen Gletscher is 10.5 km, and it is located north of the transition from Nordfjord to Moskusoksefjord. The calving front of Waltershausen Gletscher was relatively stable between 2000 and 2009, with 0.13 km ice front retreat from 2001 to 2005 and a total advance of 0.15 km between 2005 and 2008 (Seale et al., 2011). Waltershausen Gletscher and the river systems dissecting the coastal plains are the major sediment sources in Nordfjord and Moskusoksefjord. These rivers originate from local plateau ice fields and cirques glaciers that cover the mountains. The lower parts of the valleys surrounding Kejsler Franz Josef Fjord, Nordfjord and Moskusoksefjord are presently ice-free (Fig. 1c).

The bedrock geology of the study area is mainly composed of Devonian sedimentary rocks (Fig. 2), known as Old Red Sandstones (Larsen et al., 2008). To the west, Neoproterozoic to Ordovician Caledonian fold- and thrust belts comprise the bedrock geology of Strindberg Land and Andrée Land, crossed by Waltershausen Gletscher. Archean to early Neoproterozoic crystalline complexes and metasediments are also exposed in the catchment area of Waltershausen and Adolf Hoel Gletschers. To the east, Carboniferous – Cretaceous sedimentary rocks and Paleogene basalts are found south and north of Fosters Bugt, respectively (Higgins et al., 2004; Andresen et al., 2007).

The hydrographic conditions in East Greenland fjords are influenced by the East Greenland Current flowing southwards along the continental margin, transporting cold, fresh polar water and sea-ice from the Arctic Ocean. As it flows southwards, sea-ice and icebergs are added by tidewater outlet glaciers along the coast, except for between October and June when shorefast sea-ice prevents drift (Jennings and Weiner, 1996; Evans et al., 2002). Three water masses were distinguished in outer Moskusoksefjord in

August 2013 (Forwick et al., 2013; Gjelstrup, 2021); i) a warm, low saline upper surface water layer (0–15 m), ii) very cold, moderate high salinity intermediate water (~15–140 m) and iii) moderately warm, high salinity bottom water (>140 m).

2.2. Glacial history and Holocene paleoclimate

Glacial landforms mapped using bathymetric data show that several ice streams drained the GrIS via fjord systems and cross-shelf troughs during the last glacial, with the NE sector of the GrIS extending all the way to the shelf edge (Evans et al., 2002, 2009; Ó Cofaigh et al., 2004; Winkelmann et al., 2010; Funder et al., 2011; Arndt et al., 2015, 2017; Laberg et al., 2017; Arndt, 2018; Olsen et al., 2020). The timing of the onset of the deglaciation is not well established, but tentatively suggested to be indicated by a marked isotope minima on the upper continental slope around 18.4 ka cal BP (Stein et al., 1996; Evans et al., 2002) (re-calibrated in this study; for age calibration see Material and Methods chapter). Marine geophysical and geological studies of the shelf landforms suggests that the style of ice stream retreat between the NE Greenland cross-shelf troughs varied; the ice stream draining through Norske Trough (76–79° N) is inferred to have undergone a relatively continuous retreat (Arndt et al., 2017), while multiple halts/stillstands interrupted the deglaciation in Store Koldewey Trough (~76° N) (Olsen et al., 2020) and Westwind Trough (~80° N) (Arndt et al., 2017). The retreat rate in Store Koldewey Trough is proposed to have locally varied between 80 and 400 m a⁻¹ (Olsen et al., 2020).

Mega-scale glacial lineations on the seafloor east of a mid-shelf grounding-zone wedge off the coast of Kejsler Franz Josef Fjord (Evans et al., 2002; Arndt, 2018) provide evidence of a fast-flowing ice stream draining through the fjord during full-glacial conditions. This mid-shelf grounding-zone wedge has been suggested to mark both the Younger Dryas position, and the maximum LGM position (Evans et al., 2002; Arndt, 2018) (Fig. 1a). The retreat of the ice front

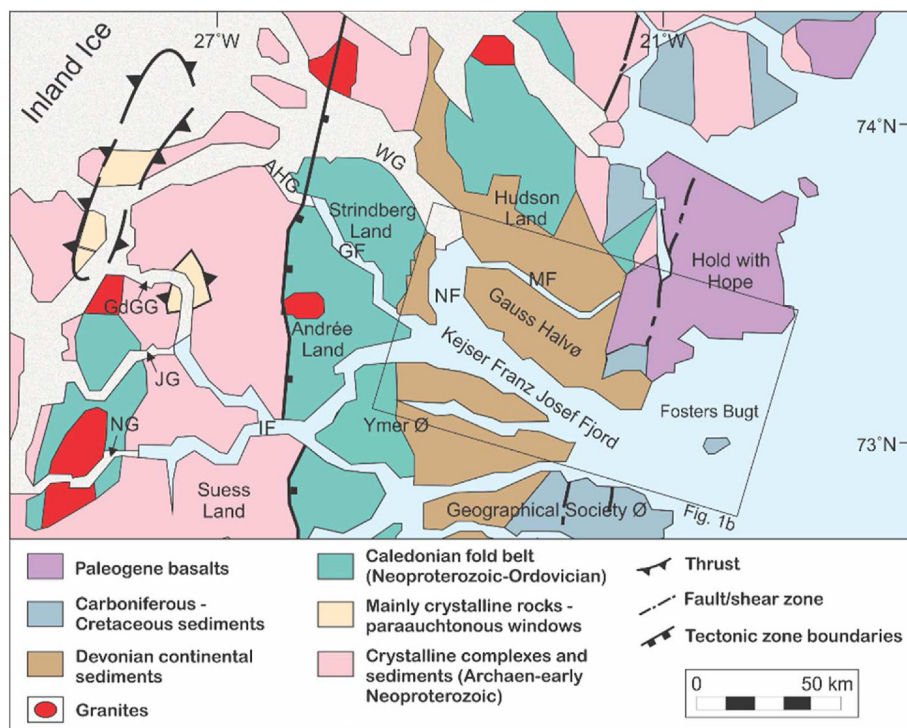


Fig. 2. Bedrock geology of the Kejsler Franz Josef Fjord region (based on Higgins et al., 2004). MF = Moskusoksefjord, N= Nordfjord, GF = Geologifjord, IF = Isfjord, WG = Waltershausen Gletscher, AHG = Adolf Hoel Gletscher, GdGG = Gerrard de Geer Gletscher, JG = Jætte Gletscher, NG = Nordenskjöld Gletscher.

is debated, with recent reviews showing that the grounding line was located in the outermost part of Kejser Franz Josef Fjord during the Younger Dryas (12.9–11.7 ka BP) (Funder et al., 2021; based on Hjort, 1979). Other studies suggests that the ice stream retreated to the fjord mouth during the Bølling/Allerød (~14.7–12.9 ka BP) warming, and that this was followed by a readvance and stabilization at a mid-shelf position during the Younger Dryas cold period (Arndt, 2018), often referred to as the Milne Land Stage moraines in NE Greenland (Funder, 1970). Further retreat in-fjord took place prior to 11.2 ka cal BP (Andrews et al., 2016).

Minimum ages reveal that the land areas surrounding Kejser Franz Josef Fjord was deglaciated in the period between 10.9 and 9.2 ka cal BP, with the outer islands (9.8 ka cal BP) becoming ice-free several hundred years later than western Ymer Ø (10.5 ka cal. BP). The occurrence of the marine shell *Mytilus edulis*, dated to ~9.5 ka cal BP, indicates an early Holocene Thermal Maximum (HTM) warming on eastern Geographical Society Ø (Wagner et al., 2010). However, lacustrine data from the same area show a delayed onset of the Holocene Thermal Maximum, around 9.0 ka BP, followed by a regional climatic cooling (the Neoglaciation) from 6.5 ka BP (Wagner et al., 2000). Recent ice-sheet models indicate that the glaciers around the Kejser Franz Josef Fjord system retreated close to its current position during the Holocene Thermal maximum (Vasskog et al., 2015). This support the results of Evans et al. (2002) who documented the presence of IRD (ice-rafted debris) throughout the middle Kejser Franz Josef Fjord sediment core, interpreted to be from iceberg calving from nearby marine-terminating glaciers, including the Waltershausen Gletscher, reaching at or near its present position during the Holocene Thermal Maximum.

The onset of the Neoglaciation coincides with an increase in IRD along the East Greenland margin, suggesting that some glaciers expanded and changed from land-terminating glaciers to tidewater glaciers (Andrews et al., 1997). Seasonable sea ice concentrations beyond the mouth of Kejser Franz Josef Fjord remained rather stable over the past 5.2 ka BP, interrupted by reduced concentrations between 2.2 and 1.3 ka BP (Kolling et al., 2017). A weak Medieval Warm Period occurred from 1 ka to 0.8 ka BP (Johnsen et al., 1992; Wagner et al., 2000). The climate thereafter cooled, reaching a culmination during the Little Ice Age (~800–100 years BP) (Levy et al., 2014), after which temperatures on Greenland increased and reached a maximum in the 1930s, followed by a new cooling period. The air temperatures have increased since the 1980s, and warming of 1.1 °C was observed at the ice sheet summit from 1991 to 2000 (Box, 2002).

3. Material and methods

3.1. Swath bathymetry data

For this study, bathymetric data have been available from two sources: 1) the IBCAO 4.0 (Jakobsson et al., 2020) providing an overview of the bathymetry of the studied fjords (Fig. 1a, c), and 2) swath bathymetry data collected during a cruise arranged within the TUNU program (Christiansen, 2012) in 2013 using *R/V Helmer Hanssen*. The swath bathymetry provides more detailed mapping in areas of low resolution of the IBCAO data, i.e., Moskusoksefjord and the inner, NE part of Nordfjord (Figs. 1c–4).

The swath-bathymetry survey was conducted using a hull-mounted Kongsberg Maritime Simrad EM 300 multibeam echo sounder, with a nominal operational frequency of approximately 30 kHz. Sound velocity profiles of the water column were recorded from CTD (conductivity-temperature-depth) measurements prior to the mapping surveys. Visualization and interpretation of the swath bathymetry data were performed using the Fledermaus

v7.8.1 3D Visualization software with a 10 × 10 m grid-cell size, whilst Global Mapper 19 was used for the IBCAO data, with a 200 × 200 m grid-cell size. The source identifier grid for the IBCAO 4.0 was examined to avoid mapping of artefacts in the data set, in particular areas with either too low or too high depth values due to poor sound profiles were omitted. From this grid and our own data, it follows that the data coverage for this study is mainly restricted to the central (deepest) part of the fjords, little or no data is covering the fjord sides except for Moskusoksefjord (Fig. 1c).

3.2. Sub-bottom profiles

High-resolution seismic CHIRP (compressed high-intensity radar pulse) profiles from Moskusoksefjord and Nordfjord were acquired using an EdgeTech 3300-HM sub-bottom profiler with a pulse frequency of 1.5–9.0 kHz and a 40 ms (ms) pulse length (for location, see Fig. 4a). The data was supplemented with sub-bottom profiles acquired using the Krupp-Atlas Parasound system (Grant and Schreiber, 1990) during the 1994 *R/V Polarstern* expedition to Kejser Franz Josef Fjord (Hubberten, 1995) (for location, see Fig. 1c). The Parasound system generated two primary frequencies of 18–23.5 kHz, generating a parametric frequency set to 4 kHz (Hubberten, 1995).

SeiSee 2.22.2 and Kingdom 2018 software were used for visualization and interpretation of the CHIRP and Parasound data, respectively. The landforms and deposits of Moskusoksefjord and Nordfjord are described from CHIRP sub-bottom profiles, whilst Kejser Franz Josef Fjord and Fosters Bugt are described by using both CHIRP and Parasound records. When calculated to sediment thickness in meters, a sediment sound velocity of 1500 ms⁻¹ is used based on the measured p-wave velocity of the collected sediment cores. Maximum penetration depth through the sediment package was ~80 m for the CHIRP and ~90–100 m for the Parasound profiles.

3.3. Sedimentological data

Five sediment gravity cores, HH13-008, HH13-009, HH13-010, HH13-011 and HH13-012, were retrieved with *R/V Helmer Hanssen* in 2013. These were complemented with three sediment gravity cores, PS2631, PS2632 and PS2633, retrieved with *R/V Polarstern* in 1994 (Hubberten, 1995; Evans et al., 2002) (Fig. 1c; Table 1).

Laboratory work on the sediment cores retrieved with *R/V Helmer Hanssen* was performed at the Department of Geosciences, UiT The Arctic University of Norway. Prior to opening, the physical properties of the sediments were measured in one-cm steps with a GEOTEK Multi Sensor Core Logger (MSCL). X-radiographs of half-core sections were acquired with a GEOTEK MSCL-XCT X-ray core imaging system. Lithological descriptions were performed from the sediment core surface, X-radiographs and line-scan color images, the latter acquired with a Jai L-107 CC 3 CCD RGB line scan camera installed on an Avaatech XRF core scanner. Sediment color was determined using the Munsell Soil Color Chart (Munsell, 2000). Qualitative element-geochemical analysis on core surfaces were performed using an Avaatech XRF Core Scanner at UiT The Arctic University of Norway. The cores were adjusted to room temperature and the cores surfaces were covered with a 4 µm ultralene film prior to scanning to avoid contamination. Instrumental settings used were 10 kV and 30 kV with a measurement distance of 10 mm. The data acquisition was carried out in two runs with a 12 and 10 mm cross-core and down-core slit sizes, respectively, using the following settings; 1) 10 kV, 1000 µA, 10 s counting time and no filter; 2) 30 kV, 2000 µA, 10 s counting time and Pd-thick filter. XRF return values for Ca, K and Fe divided over the sum of the most abundant elements (Al, Si, K, Ca, Ti, Fe and Rh) were chosen for further interpretation, reflecting the relative variations in sediment

Table 1
Locations, water depths and recoveries for the sediment gravity cores.

Core ID	Location	Latitude (°N)	Longitude (°W)	Water depth (m)	Recovery (cm)
HH13-008	Moskusoksefjord	73° 37.23'	23° 05.10'	256	226
HH13-009	Moskusoksefjord	73° 41.83'	23° 27.35'	233	283
HH13-010	Moskusoksefjord	73° 43.59'	23° 52.08'	227	486
HH13-011	Nordfjord	73° 42.51'	24° 10.17'	209	597
HH13-012	Nordfjord	73° 40.51'	24° 10.93'	210	459
PS2631	Kejser Franz Josef Fjord	73° 10.41'	22° 10.59'	430	725
PS2632	Kejser Franz Josef Fjord	73° 24.23'	23° 38.42'	504	258
PS2633	Kejser Franz Josef Fjord	73° 28.48'	24° 36.36'	283	585

provenance and composition. Granulometric analysis of material finer than 2 mm were performed with a Beckman Coulter LS 13,320 Laser Diffraction Particle Size Analyzer following the preparation method described by Dijkstra et al. (2017). Sampling was predominantly performed in intervals of 10 cm. However, the sampling distance was occasionally reduced, e.g. related to visual variations in grain-size. Particles larger than 2 mm are presented as clasts in the lithological logs.

The physical properties and granulometric analysis of the three sediment cores retrieved with R/V *Polarstern* were measured and performed by Evans et al. (2002) and Andrews et al. (2016).

New lithological descriptions and qualitative element-geochemical analysis on core surfaces (XRF; for details, see above) of the cores were performed as part of this study.

Samples of carbonate shells used for radiocarbon dating were collected and handpicked at UiT for cores HH13-008, HH13-009, HH13-011 and HH13-012, while the samples obtained in this study from cores PS2631, PS2632 and PS2633 were collected and handpicked at the Alfred Wegener Institute (AWI) in Bremerhaven, Germany. Accelerator mass spectroscopy (AMS) ¹⁴C dating was

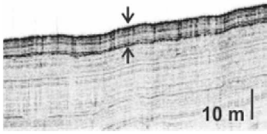
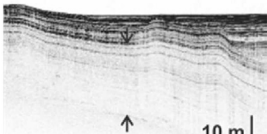
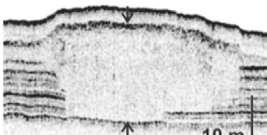
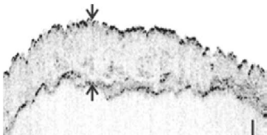
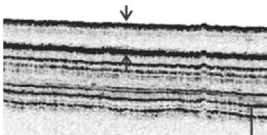
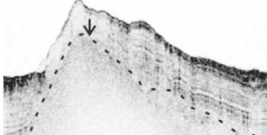
carried out at the Laboratory for Ion Beam Physics, ETH Zurich, Switzerland, and the Mini Carbon Dating System (MICADAS) facility at AWI (Table 2a). Previously published ages are from Andrews et al. (2016) and Evans et al. (2002). Age calibration was performed using the CALIB 8.2 software (Stuiver et al., 2020), applying the Marine20 calibration curve (Heaton et al., 2020) with ΔR = 0 ± 50, as recommended by Andrews et al. (2016).

All dates are presented in calibrated years before present (ka cal BP), where zero year BP is 1950 CE. Two of the radiocarbon ages represent age reversals (in cores HH13-008 and PS2633, see Table 2). They are interpreted to result from re-sedimentation and are, therefore, not considered in the further discussion. In core PS2633 the same level was dated twice using benthic foraminiferal species. One dating was performed on the species *Cassidulina neoteretis* giving an age of 7635 ¹⁴C years where the other one was performed on *Cibicides lobatulus* and showing an age of 8116 ¹⁴C years (Table 2). *C. lobatulus* is epifaunal and often lives attached to plants or hard sediment grains, hence when it is found in muddy sediment as in core PS2633, it is often reworked which may explain the older age (cf. Saher et al., 2012). Linear sedimentation rates (cm/

Table 2
(a) Radiocarbon dates and calibrated ages from the gravity cores in Moskusoksefjord, Nordfjord and Kejser Franz Josef Fjord. *Age reversal. (b) Other published and recalibrated dates from the region, ** *Mya truncata* and *Hiatella arctica*, *** *Hiatella arctica*, **** *Mya truncata* and *Hiatella arctica*.

(a) Core	Depth (cm)	Dated material	Laboratory reference	¹⁴ C age BP	Cal yr BP 1 σ range	Cal yr BP	Reference
HH13-008	114	Mixed benthic foram.	60276.1.1	1620 ± 65	913–1114	1013*	This study (ETH)
	202	<i>Buccinum hydrophanum</i>	60277.1.1	1205 ± 60	524–682	611	This study (ETH)
HH13-009	117	<i>Ostracoda</i>	60278.1.1	1790 ± 300	869–1518	1197	This study (ETH)
HH13-011	592	Mixed benthic foram.	60280.1.1	1750 ± 130	983–1287	1141	This study (ETH)
HH13-012	195	Mixed benthic foram.	60281.1.1	1295 ± 70	589–787	693	This study (ETH)
	454	Mixed benthic foram.	60282.1.1	7470 ± 130	7607–7902	7752	This study (ETH)
PS2631	99	<i>Buccinum hydrophanum</i>		1695 ± 55	977–1181	1090	Evans et al. (2002)
	390	<i>Thyasira gouldi</i>		7990 ± 210	8024–8524	8295	Evans et al. (2002)
	573	<i>Cassidulina neoteretis</i>	4494.1.1	9968 ± 92	10,679–11,031	10,838	This study (AWI)
PS2632	707	Mixed benthic foram.		10,210 ± 30	11,074–11,247	11,166	Andrews et al. (2016)
	8	<i>Cassidulina neoteretis</i>	4493.1.1	1087 ± 59	447–613	520	This study (AWI)
PS2633	97	<i>Cassidulina neoteretis</i> + <i>Islandiella helenae</i>	4495.1.1	1692 ± 55	975–1178	1087	This study (AWI)
	64	<i>Cassidulina neoteretis</i>	4496.1.1	7635 ± 75	7792–8017	7911	This study (AWI)
PS2633		<i>Cibicides lobatulus</i>	4496.2.1	8116 ± 77	8307–8543	8422	This study (AWI)
	142	<i>Cassidulina neoteretis</i> + <i>Islandiella helenae</i>	4492.1.1	8634 ± 78	8974–9250	9097*	This study (AWI)
	206	<i>Cassidulina neoteretis</i> + <i>Cibicides lobatulus</i>	4491.1.1	8376 ± 84	8590–8900	8746	This study (AWI)
(b) Latitude	Longitude	Dated material	Laboratory reference	¹⁴ C age BP	Cal yr BP 1 σ range	Cal yr BP	Reference
73° 40'	22° 00'	<i>Mya truncata</i> + <i>Hiatella arctica</i>	Lu-883	9220 ± 90	9608–9960	9804	Håkansson (1975)
73° 04.26'	23° 19.48'	Mixed benthic foram.		7495 ± 260	7502–8037	7787	Andrews et al. (2016)
73° 05.34'	19° 17.20'	<i>Portlandia fraterna</i>	AAR-2692	9560 ± 120	10,109–10,481	10,272	Evans et al. (2002)
73° 05.42'	18° 02.27'	<i>Neogloboquadrina pachyderma sin</i>	AAR-2423	13,560 ± 130	15,287–15,709	15,506	Evans et al. (2002)
72° 43.23'	22° 27.54'	Leaves, twigs	UtC-8454	8960 ± 160	9884–10,246	10,031	Wagner et al. (2000)
73° 19.35'	25° 12.23'	Bivalve	UtC-7465	9730 ± 130	10,263–10,672	10,493	Wagner and Melles (2002)
72° 53.58'	21° 57.60'	<i>Hiatella arctica</i>	AAR-8850	10,010 ± 70	10,754–11,056	10,895	Wagner et al. (2010)
73° 10.00'	21° 37.59'	Marine shells** (in situ)	K-2376	9210 ± 110	9578–9958	9794	Weidick (1976)
73° 72'	24° 62'	Marine shells*** (in situ)	K-2418	8690 ± 130	8988–9353	9156	Weidick (1976)
73° 45.00'	22° 18.00'	Marine shells/fragments****	I-9102	9205 ± 250	9486–10,132	9804	Weidick (1977)

Table 3
Seismic facies identified from CHIRP and Parasound data in Moskusoksefjord, Nordfjord, Kejser Franz Josef Fjord and Fosters Bugt.

Seismic facies	Seismic facies example	Description	Interpretation
S1a		Acoustically stratified facies with high amplitude, parallel reflections. Fills in fjord basins or drapes underlying topography.	Ice-proximal glacial marine sedimentation from suspension settling and occasional ice rafting/hemipelagic sedimentation. Episodes of gravity-flow activity and resedimentation.
S1b		Acoustically stratified facies with parallel, moderate to low amplitude reflections. Fills in fjord basins or drapes underlying topography.	Ice-proximal glacial marine sedimentation from suspension settling and occasional ice rafting/hemipelagic sedimentation. Episodes of gravity-flow activity and resedimentation.
S2		Acoustically transparent facies with lens-shaped geometry. Truncates underlying facies.	Mass-transport deposits
S3		Acoustically contorted to chaotic facies with an irregular upper surface. Overlies the acoustic basement on topographic highs or occurs along the fjord side slopes.	Reworked and homogenized sediments caused by mass-transports, gullies and iceberg scouring.
S4		Acoustically transparent to stratified facies with occasional low amplitude, parallel continuous to semi-continuous reflections. Drapes the seafloor in Kejser Franz Josef Fjord and Fosters Bugt.	Ice-distal glacial marine sedimentation from suspension settling and occasional ice rafting.
S5		Acoustically impenetrable to massive facies. The upper reflection amplitude varies spatially, whilst there is no lower reflection.	Acoustic basement, either comprising bedrock or till. Ridges are interpreted as large moraines.

ka) were calculated assuming a constant accumulation of sediments between the dated intervals (Table 3). The previously published radiocarbon ages presented in this study (Table 2) were recalibrated using the updated and extended radiocarbon calibration curves, Marine20 (Heaton et al., 2020) and IntCal20 (Reimer et al., 2020) (Table 2b).

4. Results

4.1. Seafloor geomorphology

4.1.1. Basins and ridges

Fosters Bugt, deepest north of Bontekoe Ø (up to 425 m) (Figs. 1c–3a), represent an offshore continuation of the Kejser Franz Josef Fjord system, and it can be defined as the inner part of a cross-shelf trough. The trough-fjord system narrows from 70 km in outer Fosters Bugt to 12 km in Kejser Franz Josef Fjord (between Gauss Halvø and Ymer Ø) (Fig. 1c). Several transverse ridges are located in

Fosters Bugt, and these are 32–100 m high, ~1–3.8 km wide, and are 0.7–18 km apart, and possibly extends across Fosters Bugt (Fig. 3a). Three of the ridges occur in a cluster north of Bontekoe Ø. As shown in this study, some of the ridges have an asymmetrical profile, with a steeper inner (ice-proximal) slope and a gentler outer (ice-distal) slope (Fig. 1, see also “Seismostratigraphy” below).

The bathymetry of Kejser Franz Josef Fjord progressively deepens inward from ~330 m at the fjord mouth to 550 m close to the transition to Nordfjord (Figs. 1c–3a). The fjord contains two main basins that are separated by an area of shallower seafloor containing several ridges. The ridges are 0.38–2.8 km wide, have reliefs of 35–84 m and are spaced 2–12 km apart. They are possibly fjord-transverse ridges, although this cannot be confirmed from the present data. Fjord-transverse ridges are identified at the transition from Kejser Franz Josef Fjord to Nordfjord, Geologifjord and Eleonores Bugt (Fig. 3a), ranging between 2.3 and 4 km width and 32–320 m reliefs.

The water depths in Nordfjord shallows from ~380 m to ~100 m

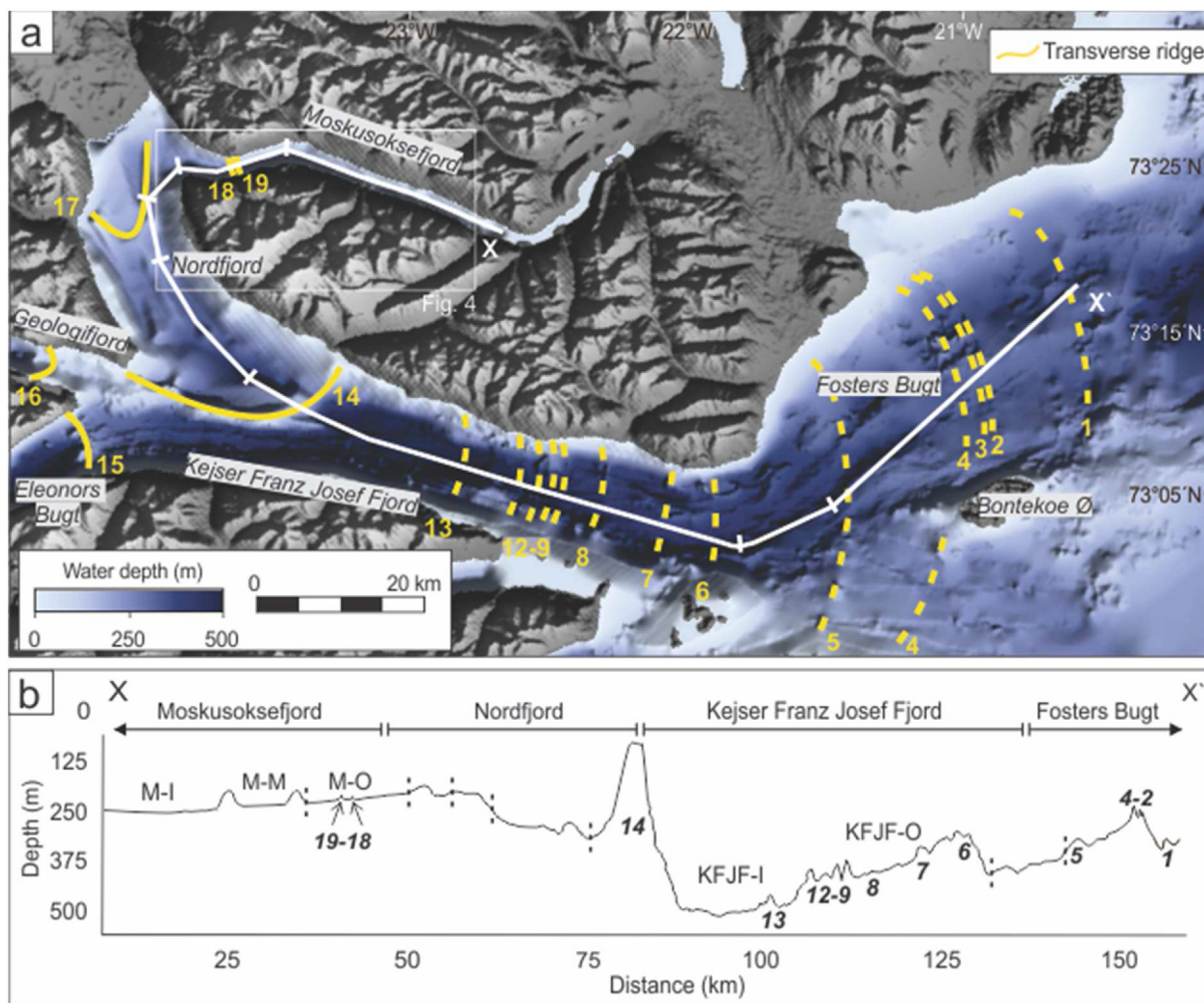


Fig. 3. Bathymetry of the Keiser Franz Josef Fjord system. (a) IBCAO v. 4.0 (Jakobsson et al., 2020) with mapped transverse ridges. White line shows the location of the bathymetric profile shown in (b). The smaller cross-lines along the profile corresponds to the dotted vertical lines in (b). Transverse ridges are marked with yellow lines and numbered. (b) Bathymetric profile of the study area. M-I = Inner basin of Moskusoksefjord, M-M = Middle basin of Moskusoksefjord, M-O = Outer basin of Moskusoksefjord, KFJF-I = Inner basin of Keiser Franz Josef Fjord, KFJF-O = Outer basin of Keiser Franz Josef Fjord. The profile was produced using a combination of IBCAO v. 4.0, swath bathymetry and sub-bottom profiles (CHIRP and Parasound). The dotted vertical lines along the profile show where the profile orientation changes in (a). (For interpretation of the references to color in this figure legend, the reader is referred to the Web version of this article.)

towards the terminus of Waltershausen Gletscher. The inner ridge, located closest to the present-day glacier front of Waltershausen Gletscher, has a ~70 m relief and ~2.6 km width.

Three basins are identified in Moskusoksefjord (Figs. 3b–4a). The maximum depths of the basins progressively increases from the outer (closest to Waltershausen Gletscher, 237 m) to the inner basin (260 m). Relatively large deltas prograde into the fjord from both sides, as detailed below. Deltas form thresholds at 216 m and 210 m water depth, separating the outer- and middle- and inner- basins, respectively.

Two transverse ridges are identified in the outer basin of Moskusoksefjord (Ridge 18 and 19; Figs. 3–4a). Ridge 19 stretches 1.3 km in a general S–N direction, sloping gently towards north. Its width narrows from 800 m in the south to 400 m in the north, whilst its height decreases from 15 m to 3 m. A cross-profile shows that this ridge is symmetric (Fig. 5a). Ridge 18 is > 770 m long and NNE to SSW oriented. The width of the ridge varies between 210 m in the upper part, to almost 300 m in the lower part. Whereas the gradient of the in-fjord facing slope exceed 30°, the out-fjord slope

gradient is ~20°. Both ridges are partly buried in the central parts of the fjord.

The internal structure of the ridges in all three fjords is acoustically transparent to massive (Fig. 6; Table 4). Based on their overall form, steeper in-fjord and slightly more gently dipping out-fjord for some of them, and their internal acoustic signature (Ridges 1, 2, 4, 9, 12, 14, 18 and 19), the ridges are interpreted to represent moraines, marking the positions of stillstands of the grounding-line, either formed during a stepwise deglaciation or a Holocene ice re-advance, as will be further discussed below. For some of the other ridges a bedrock sill origin cannot be excluded although we find this less likely as the bedrock in this area is Devonian sandstone, less resistant to erosion compared to the crystalline bedrock to the west. Based on this, it is less likely to find bedrock sills in this area. A notable exception is Fosters Bugt where intrusion of basalt has been identified to the north, possibly extending into the fjord-mouth trough, for instance in the area of Ridge 3 (Fig. 3 and 6).

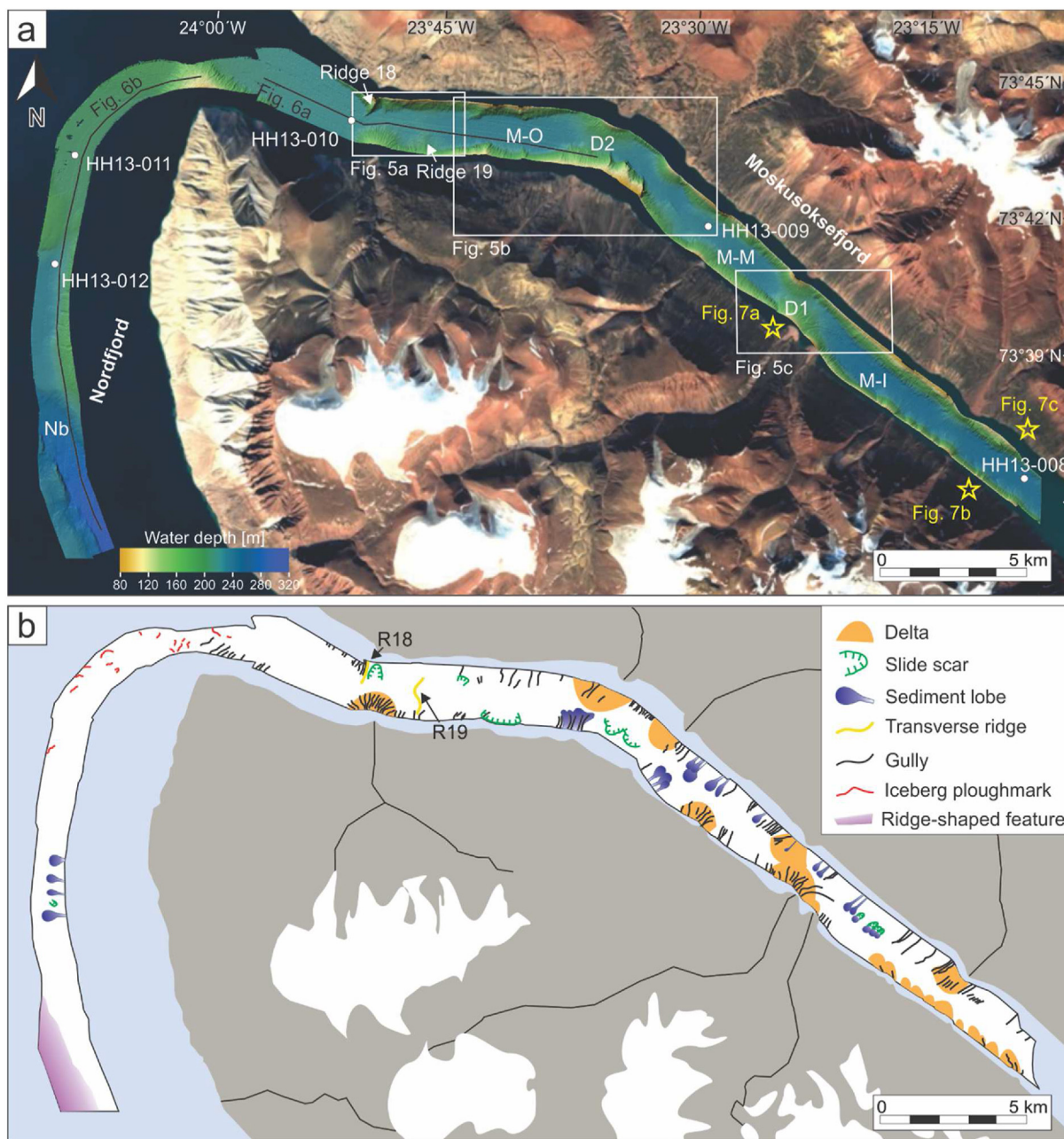


Fig. 4. (a) Shaded swath bathymetry data. White circles indicate the location of the sediment gravity cores retrieved on R/V Helmer Hanssen in 2013, whilst yellow stars show the locations of the images in Fig. 7. M-I = Inner basin of Moskusoksefjord, M-M = Middle basin of Moskusoksefjord, M-O = Outer basin of Moskusoksefjord, Nb = Nordfjord basin, D1 = Deltas separating inner- and middle basins of Moskusoksefjord, D2 = Delta separating middle- and outer basins in Moskusoksefjord. Background image from Copernicus Sentinel Data (2020). (b) Map of the interpreted landforms identified in (a). Glaciers and major river systems are indicated. (For interpretation of the references to color in this figure legend, the reader is referred to the Web version of this article.)

4.1.2. Deltas

Fan shaped protuberances of different sizes are observed along the fjord sides, mainly as continuations of rivers draining from plateau ice fields and cirques (Figs. 4 and 5). Some of them also include raised shorelines, and up to five levels have been identified on land (Fig. 7a). Most of the protuberances (15) are located along the S-SW fjord sidewall, while four are located on the N-NE side. The features have maximum widths ranging from 350 m to 2.3 km.

Their slope gradients exceed 20° in the upper, coast-proximal parts, decreasing to a gradient <10° in the distal fan areas, producing generally concave profiles. Gullies (for details see below) dissect the lower parts of the features (Fig. 5c).

Based on their geometries, the protuberances are interpreted to be deltas, and based on their relatively steep slopes and proximity to sediment sources on land, they likely consist of coarse-grained sediments (Figs. 4 and 5). These are therefore typical Gilbert

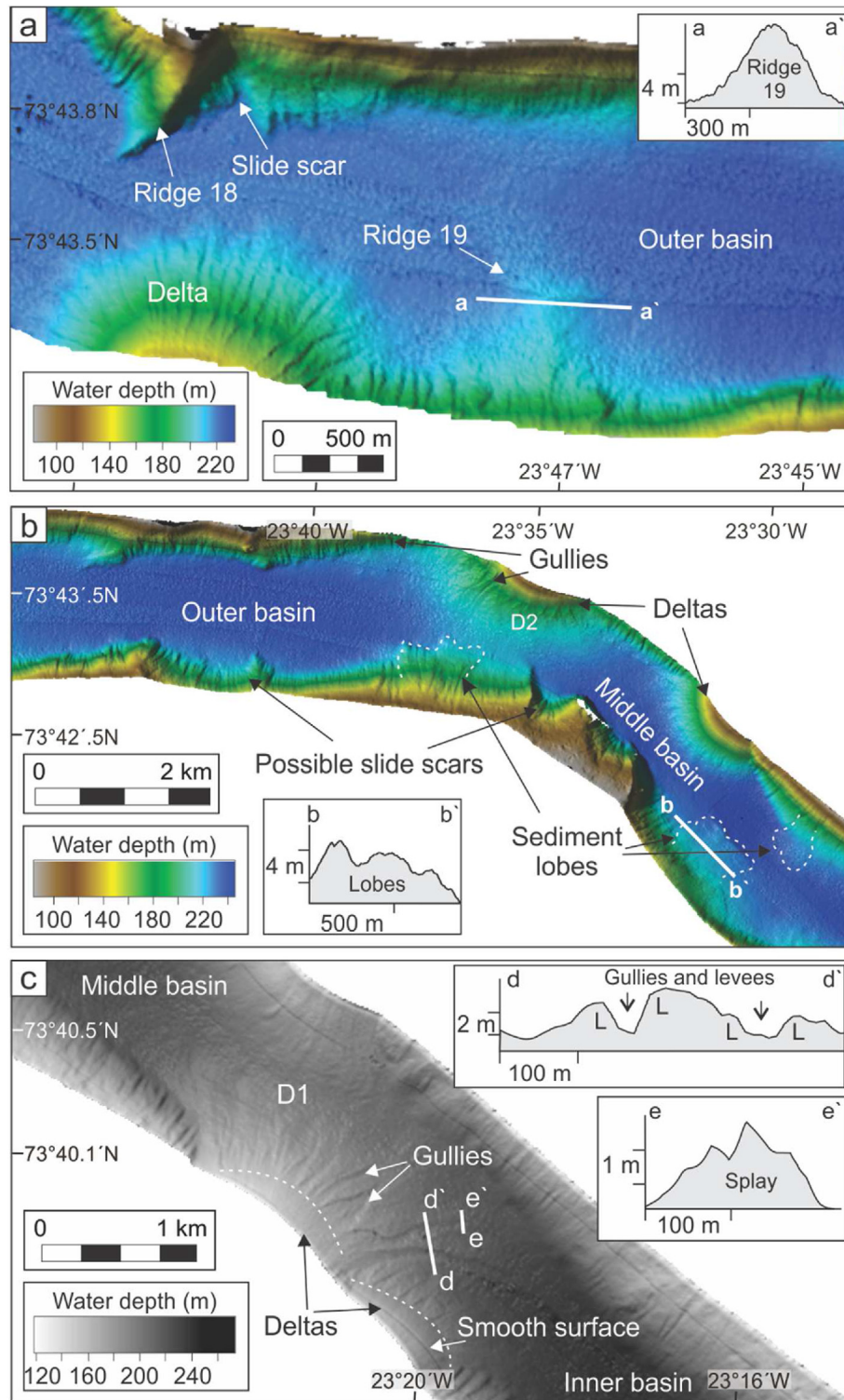


Fig. 5. Grayscale and color shaded bathymetry images with examples of seafloor geomorphology and profiles in Moskusoksefjord (see Fig. 4 for location). (a) Delta and two ridge segments at the fjord mouth. Profile a-a' shows ridge 19. (b) Bathymetry of the outer/middle basin area, including possible slide scars, sediment lobes, deltas and gullies. D2 = Delta separating middle- and outer basins in Moskusoksefjord. Profile b-b' shows three superimposed sediment lobes. (c) Two river deltas off the southwestern shore separating the middle and inner basins with accompanying gullies. D1 = Deltas separating inner- and middle basins of Moskusoksefjord. Profile d-d' crosses two gullies (indicated by arrows) with adjoining levees (L), whilst profile e-e' spans across a splay. (For interpretation of the references to color in this figure legend, the reader is referred to the Web version of this article.)

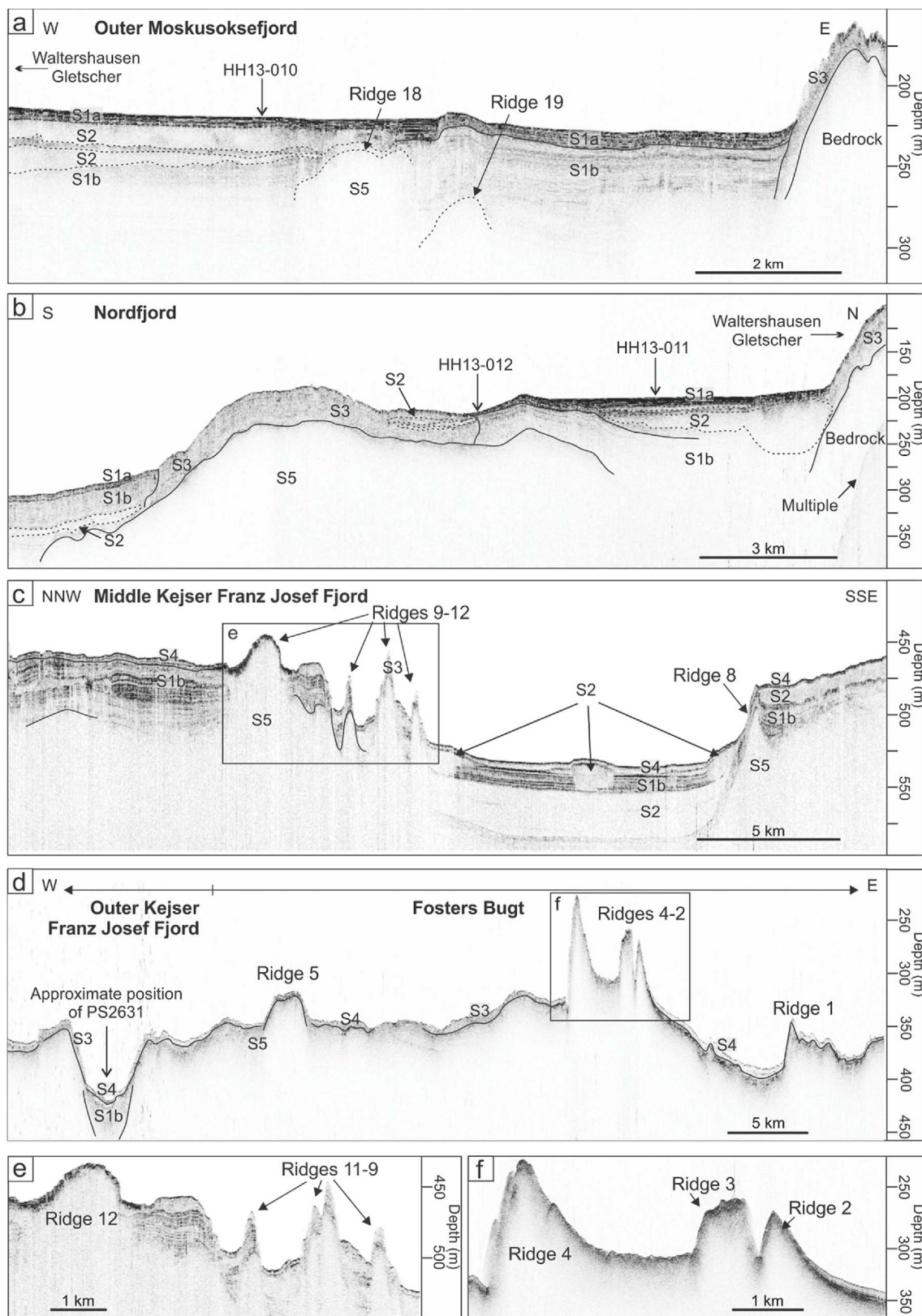
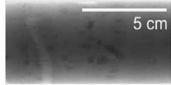
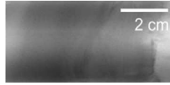
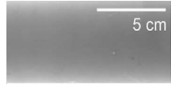
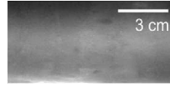
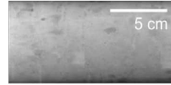
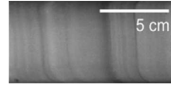
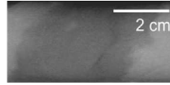


Fig. 6. Selected CHIRP and Parasound sub-bottom profiles along (a) outer Muskusoksefjord, (b) Nordfjord, (c) middle Kejser Franz Josef Fjord and (d) outer Kejser Franz Josef Fjord – Fosters Bugt. Fig. (a), (b) and (d) are CHIRP profiles, (c) is Parasound. The interpreted seismic facies are indicated. For locations, see Figs. 1c–4a. (e) Part of the Parasound sub-bottom profile in Middle Kejser Franz Josef Fjord showing interpreted moraine ridges. (f) Part of the CHIRP sub-bottom profile in Fosters Bugt showing interpreted moraine ridges.

Table 4
Overview of the lithofacies physical and compositional characteristics. Sedimentary processes and environment are inferred.

Lithofacies	1 Laminated mud with dispersed clasts	2 Laminated mud	3 Bioturbated mud with dispersed clasts	4 Massive mud with lenses of sand and dispersed clasts	5 Sandy mud with clasts	6 Laminated mud with lenses of sand and dispersed clasts	7 Sandy mud
X-Radiograph							
Color (Munsell Soil Color Chart)	Gray (5Y 5/1)	Olive gray (5Y 4/2)	Dark grayish brown (2.5Y 4/2)	Dark gray (5Y 4/1)/ Reddish brown (5 YR 4/3)	Dark grayish brown (2.5Y 4/2)	Reddish brown (5 YR 4/3)/ Pinkish gray (5 YR 6/2)/ Gray (5Y 5/1) to olive gray (5Y 4/2)	Dark reddish brown (5 YR 3/2)/Dark grayish brown (2.5Y 4/2)
Upper boundary	Erosional /Gradational	Sharp	Seafloor	Erosional/Sharp	Seafloor	Erosional	Sharp
Lower boundary	N/A	Erosional	Gradational	Gradational	Erosional	Sharp	Erosional
Bioturbation	Very low	Absent	Intense	Low	Absent	Low to moderate	Absent
Clast amounts	Low to moderate	Absent	Low	Moderate	High	Low to moderate	Absent
Magnetic susceptibility (10 ⁻⁵ SI)	50–60	60–90	50–170	15–65	60–100	20–85	10–55
Wet bulk density (g/cm ³)	1.7–2.0	~2.0	1.36–1.70	1.6–1.8	1.8–2.15	1.7–1.8	1.65–2.1
Ca/Sum	0.07–0.3	0.12–0.17	0.05–0.15	0.05–0.14	0.07–0.17	–0.11	0.10–0.18/~0.2
K/Sum	0.10–0.16	0.11–0.15	0.12–0.15	0.10–0.16	–0.14	–0.13	0.13–0.18/~0.08
Fe/Sum	0.27–0.46	0.27–0.39	0.39–0.51	–0.42	0.35–0.45	–0.43	0.35–0.44/0.18–35
Sedimentary processes and environment	Ice-proximal glacimarine sedimentation; suspension settling from glacial meltwater plumes, episodic calving events	Ice-proximal glacimarine sedimentation; suspension settling from glacial meltwater plumes	Ice-distal glacimarine sedimentation dominated by suspension settling and episodic ice rafting	Ice-distal glacimarine sedimentation dominated by suspension settling and episodic ice rafting, together with gravity-flow activity	Mass-transport	Ice-proximal glacimarine sedimentation; suspension settling from glacial meltwater plumes, episodic calving events, together with gravity-flow activity	Mass-transport /Density currents in an ice-proximal environment

deltas, which often form in steep-sided fjords where a river enters the fjord over a longer period of time (Bogen, 1983; Gales et al., 2019). Raised parts including shorelines implies that the delta progradation was influenced by a stepwise relative sea-level fall over a longer period (c.f. Corner, 2006). If correct, this would most likely have initiated immediately after the Early Holocene deglaciation of this area, implying that the deltas have developed from the deglaciation to the present.

4.1.3. Submarine gullies

Numerous downslope oriented, straight to curvilinear incisions have been observed along the fjord sides of Moskusoksefjord. Two main types have been identified, the first in association with deltas, the other represents a continuation from subaerial gullies originating from mountain incisions or slide scars dominated by coarse-grained sediments (Figs. 4, 5 and 7). Both types of incisions are up to 170 m wide, <8 m deep and can be followed for up to 2.2 km. Most of the features have flanking levees and typically appear as single incisions. However, in some cases, two incisions merge downhill into one feature, and in other cases, single incisions splits into two individual features. Some of the incisions end downslope with thin splays that are usually less than 3 m thick (Fig. 5c).

The incisions are interpreted to be submarine gullies (Figs. 4 and 5). The gullies associated with deltas are characteristic features of Gilbert-type deltas, formed by turbidity currents generated by coarse bedload avalanches or slope failures (Gales et al., 2019). The second type of gullies, representing the marine part of subaerial gullies on land, are interpreted to be produced by annual snow-fed meltwater flow. In cases where the downslope flow of sediment masses exceeds the width of the gullies, levees are formed by overbank flood sedimentation.

4.1.4. Slide scars and sediment lobes

Amphitheater-shaped incisions that are 0.5–1.3 km wide are found in the outer basin of Moskusoksefjord (Figs. 4–5a), whilst smaller features (50–200 m wide) are located on the E-NE slope in the middle and inner basins (Figs. 4–5b), i.e. wider incisions occur where the fjord wall gradient is lower. The depths of the incisions range from 3 to 30 m, and headwall gradients vary from 14° to 30°. Some of the incisions are more distinct than others, i.e. some appear to be partly buried by sediments. Similar incisions are seen some tens of meters above present sea level (Fig. 7). One incision is also identified in Nordfjord (Fig. 4).

Several of the incisions have associated sediment lobes on the fjord floor. These vary in both size and character and are often found as sets of several superimposed lobes (Fig. 5b). Individual lobes have lengths of 100–550 m, maximum widths from 80 to 850 m and they are up to 8 m thick. In the CHIRP sub-bottom data the lobed shaped deposits has an acoustically semi-transparent facies with a few chaotic internal reflections, and the base of the deposits truncate underlying reflections (facies S2). (Fig. 6; Table 4). Only the incisions in the inner basin of Moskusoksefjord have visible lobe shaped deposits directly downslope of the features, indicating that the potentially associated lobes in the outer basin of Moskusoksefjord and in Nordfjord must have been buried.

The incisions are interpreted to be slide scars formed by failure of deposits along fjord sidewalls (Figs. 4 and 5a, b and 7), a frequently observed phenomenon in fjords elsewhere (e.g. Bøe et al., 2000; Forwick and Vorren, 2012; Bellwald et al., 2019). The lobe shaped deposits are interpreted to be their associated mass-transport deposits based on their geometries and internal seismic signatures, as well as their locations at the bottom of steep slopes, often downslope from the slide scars (Figs. 4 and 5a, b). The mass-transport deposits are thickest in the outer basin of Moskusoksefjord, implying a higher sedimentation rate here, likely

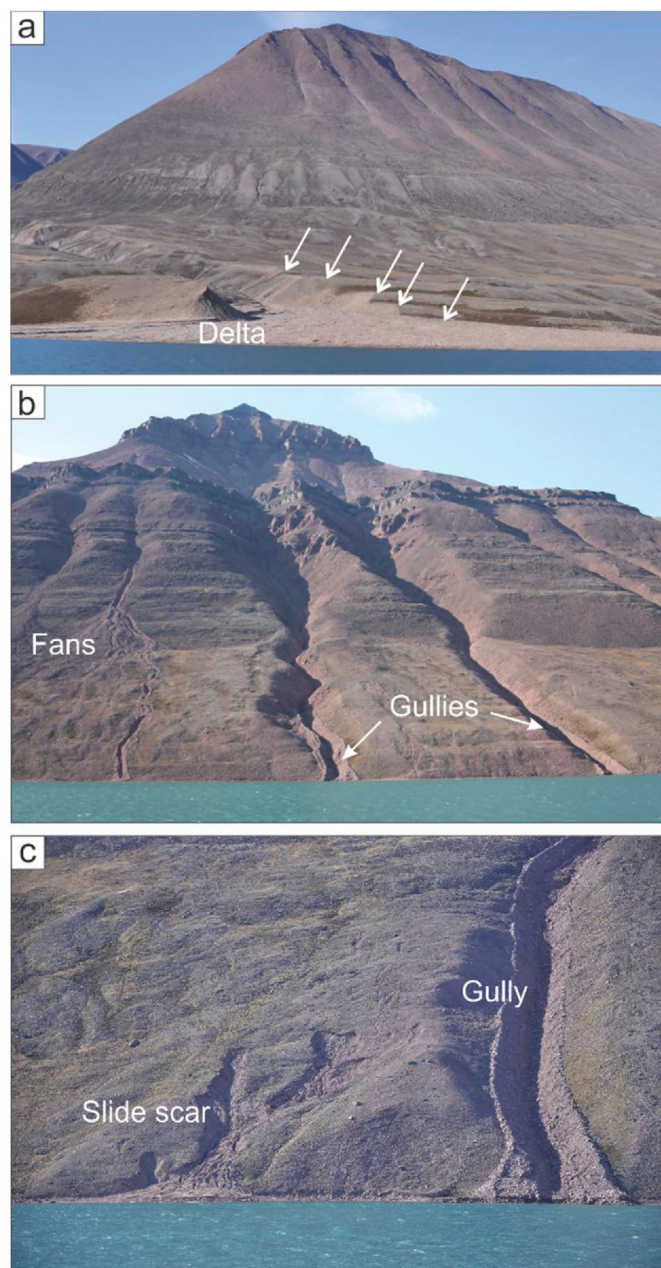


Fig. 7. Pictures from Moskusoksefjord taken in August 2013, showing various sedimentary systems. a) Gilbert-type delta. Five levels of raised shorelines are indicated with white arrows. The delta is marked as D1 in Fig. 4a). The mountain in the background is 1260 m high. b) Subaerial alluvial fans and gullies. c) Slide scar and subaerial gully. See Fig. 4a for locations.

related to the proximity to the Waltershausen Gletscher.

4.2. Seismostratigraphy

Five seismostratigraphic facies (S1–S5) are identified from CHIRP and Parasound data in Moskusoksefjord, Nordfjord and Keiser Franz Josef Fjord. The acoustic characteristics and interpretations are presented in Table 4 and follows the terminology of Mitchum et al. (1977) and others as detailed below.

4.2.1. Seismic facies S1a and S1b (acoustically stratified)

Seismic facies S1a and S1b consist of parallel to sub-parallel

internal reflections with high continuity (Fig. 6; Table 4), and we term this as “acoustically stratified”, in accordance with Dowdeswell et al. (1994), Evans et al. (2002) and Plassen et al. (2004). The facies is present in all three fjords, either as a ponded basin infill with onlapping reflections at the basin sides or draping underlying topography in the central parts of the fjords (Fig. 11). Whereas the facies generally occurs as the uppermost facies in Moskusoksefjord and Nordfjord, it is overlain by facies S4 in Kejser Franz Josef Fjord. Seismic facies S1 was sampled by all sediment cores from Moskusoksefjord and Nordfjord, in addition to cores PS2631 and PS2633 from Kejser Franz Josef Fjord (Fig. 11). Facies thickness varies with between 7 and 22 m when overlying topographic highs, whereas it exceeds the penetration depth in the basins. Lens- or lobate-shaped acoustic transparent sediment bodies (facies S2) occur occasionally within facies S1. The facies is divided into two sub-facies based on a distinct change in the acoustic signature going from high amplitude reflections in sub-facies S1a to moderate to low amplitude reflections in sub-facies S1b (Table 4). Sub-facies S1a lies conformable above S1b. Facies S1 corresponds to acoustic facies 1a in Evans et al. (2002).

4.2.2. Seismic facies S2 (acoustically transparent)

S2 is an acoustically transparent facies (“reflection free”, sensu Mitchum et al., 1977). It has a discontinuous and undulating upper boundary and a lower boundary typically truncating underlying reflections (Table 4). The facies occur as lensoidal bodies within facies S1 that are up to 55 m thick, and pinches out laterally (Figs. 6 and 11). The facies corresponds to acoustic facies 2 in Evans et al. (2002).

4.2.3. Seismic facies S3 (acoustically chaotic)

An acoustically contorted to chaotic signature with low internal reflection continuity characterizes facies S3 (Figs. 6 and 11; Table 4). The facies has a highly irregular, high amplitude surface reflection with diffraction hyperbolas on steep slopes and a locally diffuse, low amplitude basal reflection. Its thickness varies, with a maximum thickness of 17 m. It lies unconformable above facies S5. Facies S3 is located along the fjord side slopes and on topographic highs (Fig. 11). This facies corresponds to acoustic facies 3 in Evans et al. (2002).

4.2.4. Seismic facies S4 (acoustically transparent to stratified)

Facies S4 is acoustically transparent to stratified (Table 4). The facies drapes the seafloor in large parts of Kejser Franz Josef Fjord and Fosters Bugt, conformably overlying facies S1 or S2 (Figs. 6 and 11). The facies has a high amplitude surface reflection and occasional internal parallel, continuous to semi-continuous reflections of low amplitude. The sediment drape is generally 1.5–2 m thick and up to 5 m thick in topographic lows. Sediment cores PS2631, PS2632 and PS2633 penetrated the facies (Fig. 6b and c and 11). This facies corresponds to acoustic facies 4 in Evans et al. (2002).

4.2.5. Seismic facies S5 (acoustically impenetrable to transparent)

Facies S5 represents an acoustically impenetrable to transparent facies (Table 4). Its upper reflection has a spatially varying amplitude, and there is little to no penetration of the acoustic signal below. The facies occurs at various depths in all three fjords (Figs. 6 and 11). It is generally overlain by facies S1 or S3, but locally forms ridges that crop out on the seafloor. The ridges are up to 80 m high, less than 2 km wide and occur in clusters near the fjord mouth, as well as in middle of Kejser Franz Josef Fjord, i.e. where the fjord is at its narrowest.

4.3. Lithological facies

A transect of eight sediment cores were analyzed; three in Kejser Franz Josef Fjord, two in Nordfjord and three in Moskusoksefjord (Fig. 1; Table 1). The cores were divided into seven lithofacies (Figs. 8–10; Table 5) based on lithology, observed structures, element geochemistry and physical properties, and are found to be dominated by bioturbated, massive, laminated and sandy mud with dispersed clasts. Below, we describe the facies in their order of appearance, starting with the bottom facies in the outermost core in Kejser Franz Josef Fjord.

4.3.1. Lithofacies 1 (laminated mud with dispersed clasts)

Lithofacies 1 is present in the outer part of the study area, in the lower parts of cores PS2631 and PS2633 (Fig. 8). The sediment cores penetrated seismic facies S1 (Fig. 11), consisting of stratified sediments. The lithofacies consists of >155 cm thick gray (5Y 5/1) laminated mud with dispersed clasts (Table 5). In core PS2631 the lithofacies has an erosional upper boundary underlying lithofacies 2, whereas in core PS2633 the boundary with the overlying lithofacies 4 is gradational. The laminated sediment has a generally low magnetic susceptibility ($50\text{--}60 \times 10^5$ SI). The Ca/sum and Fe/sum ratios show opposite trends, with the highest Ca/sum and lowest Fe/sum in core PS2631. Bioturbation is low and the clast content is low to moderate. The wet bulk density is uniform.

4.3.2. Lithofacies 2 (laminated mud)

Lithofacies 2 is found exclusively in core PS2631 from outer Kejser Franz Josef Fjord (Fig. 8). It consists of olive gray (5Y 4/2) laminated mud absent of clasts and bioturbation (Table 5), with a thickness of 14 cm. The boundary with the underlying lithofacies 1 is erosional, whereas the upper boundary to lithofacies 3 is sharp. The wet bulk density is high. The lithofacies is characterized by a sudden change in the magnetic susceptibility, wet bulk density and Ca/sum and Fe/sum ratios relative to the underlying gray laminated mud with dispersed clasts (lithofacies 1).

4.3.3. Lithofacies 3 (bioturbated mud with dispersed clasts)

Lithofacies 3 contains dark grayish brown (2.5Y 4/2) massive mud with dispersed clasts, and is characteristic of the upper 520 cm of core PS2631 and the entire core PS2632 (Fig. 8) (i.e. the transparent to stratified sediments draping the outer and middle Kejser Franz Josef Fjord (facies S4)) (Fig. 11). The lithofacies is intensely bioturbated and has low clast amounts (Table 5). The lithofacies is further characterized by uniform geochemical elements and variable magnetic susceptibility ($55\text{--}160 \times 10^5$ SI) and wet bulk density. The magnetic susceptibility is mainly higher in this facies than for facies 1–2, with a decreasing normal consolidation trend in core PS2631 and an increasing trend, possibly due to higher clast content towards the top, in core PS2632. The lowest wet bulk density occurs towards the top of core PS2631 (down to 1.36 g/cm^3).

4.3.4. Lithofacies 4 (massive mud with lenses of sand and dispersed clasts)

Lithofacies 4, consisting of massive mud with lenses of sand and dispersed clasts, is found in cores PS2633 and HH13-008 from inner Kejser Franz Josef Fjord and innermost Moskusoksefjord (Figs. 8 and 10). In core PS2633, the lithofacies is 150 cm thick and dark gray (5Y 4/1) in color (Table 5). It lies directly above lithofacies 1 and under lithofacies 3, with gradational and erosional boundaries, respectively. In core HH13-008, the lithofacies is > 85 cm thick, reddish brown (5 YR 4/3), and found at the base of the core

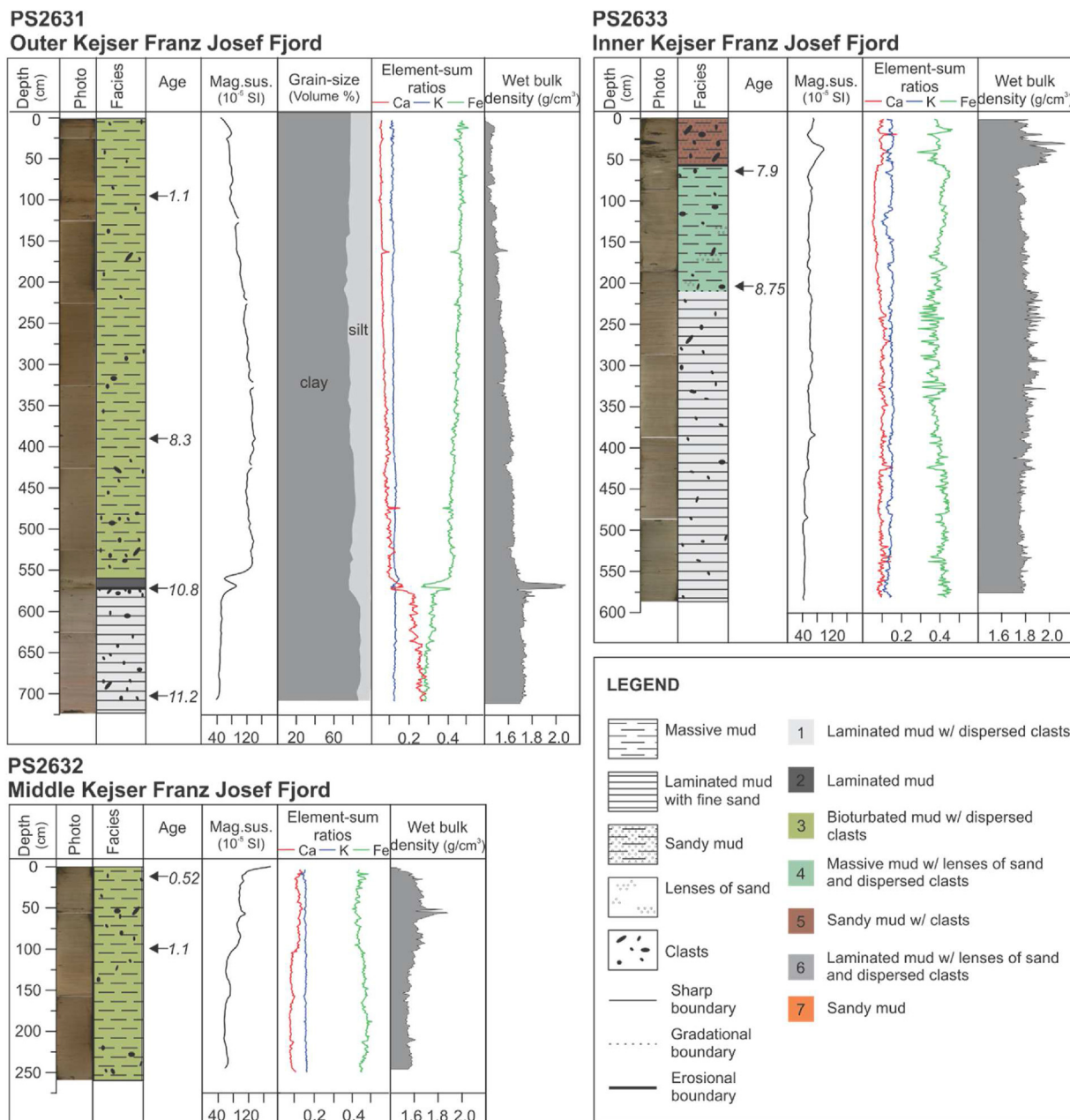


Fig. 8. Composite logs of core PS2631, PS2632 and PS2633 retrieved from Kejsjer Franz Josef Fjord, showing lithofacies, line-scan images, grain-size distribution, physical properties and XRF core-scanning geochemistry. The latter presents the ratio of selected elements over the eight most abundant elements. Calibrated radiocarbon ages, presented in calibrated years before present, are indicated with arrows. Core locations are shown on Fig. 1.

(Table 5). It has a sharp boundary to the overlying lithofacies 6. Magnetic susceptibility is low in both cores (15–65 × 10⁵ SI), whereas the wet bulk density and geochemical elements show little variation. The lithofacies has little bioturbation and a moderate number of clasts.

4.3.5. Lithofacies 5 (sandy mud with clasts)

Lithofacies 5 is found exclusively at the top of core PS2633 in inner Kejsjer Franz Josef Fjord (Fig. 8, Table 5), recovered from an acoustically transparent sediment body (facies S2) (Fig. 11). The lithofacies is 60 cm thick and consists of a dark grayish brown (2.5Y 4/2) sandy mud with a high number of clasts. Bioturbation is

absent. It has an erosional lower boundary, overlying lithofacies 7. The lithofacies has a relatively high wet bulk density (1.8–2.15 g/cm³), corresponding with a peak in magnetic susceptibility. The Ca/sum and Fe/sum ratios have similar values as the laminated mud with dispersed clasts (lithofacies 1) further downcore.

4.3.6. Lithofacies 6 (laminated mud with lenses of sand and dispersed clasts)

Lithofacies 6, consisting of laminated mud with lenses of sand and dispersed clasts, is present in the cores retrieved from stratified sediments in Moskusoksefjord and Nordfjord (facies S1a) (Figs. 6, 9 and 11). The laminated mud is characterized by frequent color

changes, alternating between reddish brown (5 YR 4/3) and pinkish gray (5 YR 6/2) in inner Moskusoksefjord, gray (5Y 5/1) and pinkish gray (5 YR 6/2) in middle Moskusoksefjord and gray (5Y 5/1) to olive gray (5Y 4/2) in outer Moskusoksefjord and Nordfjord (Table 5). The lithofacies is interbedded by layers of lithofacies 7. Bioturbation and clast content is low to moderate, with a higher clast number in the cores located furthest away from the modern

glacier front of Waltershausen Gletscher. The wet bulk density and magnetic susceptibility values are uniform, with a slight increase in the density from normal sediment compaction. The geochemical elements show little variation, with small peaks following the lithology.

4.3.7. Lithofacies 7 (sandy mud)

Lithofacies 7 is present in the core from inner Nordfjord (Fig. 9) and all three cores from Moskusoksefjord (Fig. 10). The lithofacies consists of fining upwards sandy mud, absent of clasts and bioturbation. It occurs as layers within lithofacies 6, with an erosional lower boundary and a sharp upper boundary. Individual layers are up to 95 cm thick. In inner and middle Moskusoksefjord, these layers are dark reddish brown (5 YR 3/2) in color, whereas they are dark grayish brown (2.5Y 4/2) in outer Moskusoksefjord and Nordfjord, respectively. High and slightly increasing wet bulk density from normal sediment compaction and low and uniform magnetic susceptibility and iron values characterize the lithofacies, with the lowest iron values in all three fjords occurring within the layers containing dark grayish brown sandy mud.

4.4. Correlation of seismostratigraphy and lithological facies

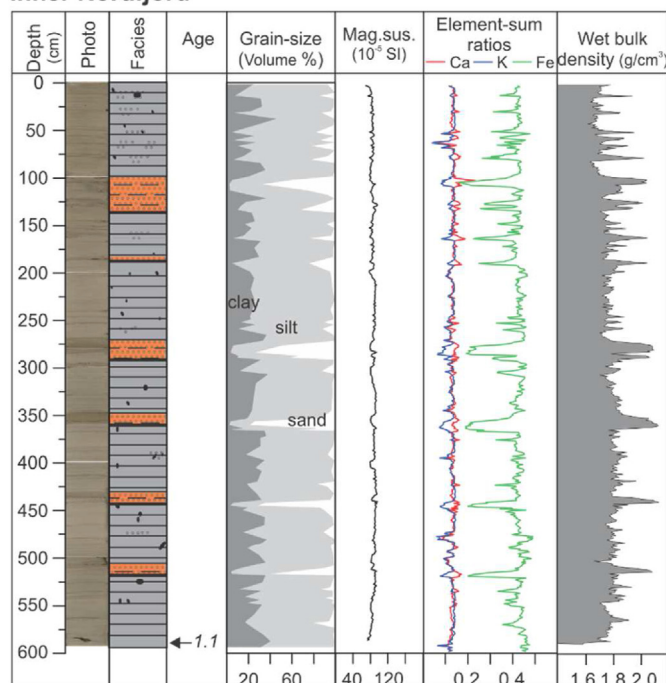
The infilling and draping seismic facies S1, comprising laminated mud with dispersed clasts and layers of sand (lithofacies 1, 2 and 6), is interpreted to represent ice-proximal sedimentation. The sedimentation includes suspension settling from glacier-margin derived turbid meltwater plumes (overflows) and episodes of rafting by icebergs and/or sea-ice, together with turbidity current activity (underflows). In comparison, seismic facies S4 has a transparent character, a draping geometry in Kejser Franz Josef Fjord system some distance from the present-day glacier front, and it consists of sandy mud. Altogether, this indicates a more ice-distal environment with more stable conditions than in facies S1 (cf. Hogan et al., 2016; Prothro et al., 2018).

The sediment cores retrieved in Kejser Franz Josef Fjord are therefore interpreted to mark the transition from an ice-proximal to an ice-distal environment, in conformity with Evans et al. (2002). The high amount of suspension settling from glacial meltwater probably dominates the iceberg-dropped component within the fjords, leading to an apparent dilution of ice-rafted debris out-fjord (Boulton, 1990).

Seismic facies S3, with an irregular upper surface and location on topographic highs and fjord side slopes, is interpreted to be seabed irregularities generated by mass-transports and turbidity channels within Moskusoksefjord and Nordfjord, whilst in the central parts of Kejser Franz Josef Fjord the irregularities are inferred to be a product of intense iceberg scouring (cf. Evans et al., 2002). Scouring of the sea floor by iceberg keels leads to reworking and homogenization of the sediments (Ó Cofaigh and Dowdeswell, 2001), thus causing a chaotic seismic signature.

The acoustic transparent signature and lensoidal geometry of facies S2, together with the erosive base of the facies are characteristic of mass-transport deposits (cf. Hjelstuen et al., 2009). The facies locations in the proximity to active river deltas, steep fjord slopes and Waltershausen Gletscher indicate a high sediment input and subsequent mass failing, thus, supporting that these deposits are related to mass-transport activity and/or density-currents (lithofacies 5 and 7). The impenetrable to massive facies S5, characteristic of moraines ridges in the study area, is suggested to represent the acoustic basement, comprising bedrock and/or subglacial till (cf. Forwick and Vorren, 2010).

HH13-011 Inner Nordfjord



HH13-012 Outer Nordfjord

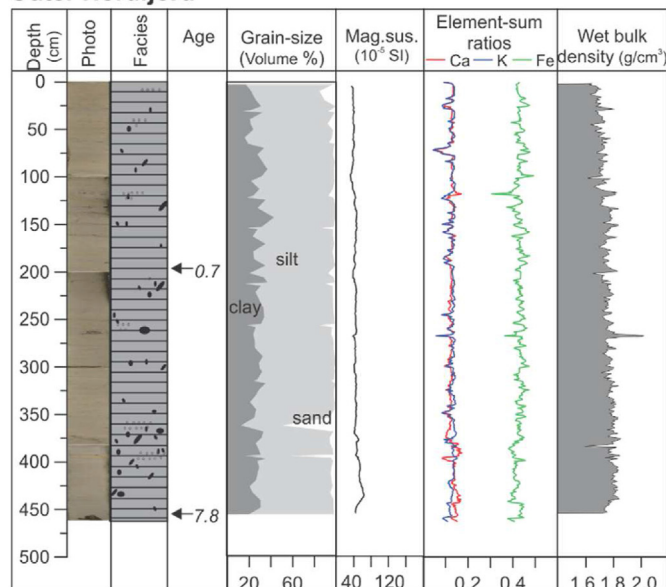


Fig. 9. Composite logs of core HH13-011 and HH13-012 retrieved from Nordfjord, showing lithofacies, line-scan images, grain-size distribution, physical properties and XRF core-scanning geochemistry. The latter presents the ratio of selected elements over the eight most abundant elements. See Fig. 8 for legend to the lithofacies. Calibrated radiocarbon ages, presented in calibrated years before present, are indicated with arrows. Core locations are shown on Fig. 1.

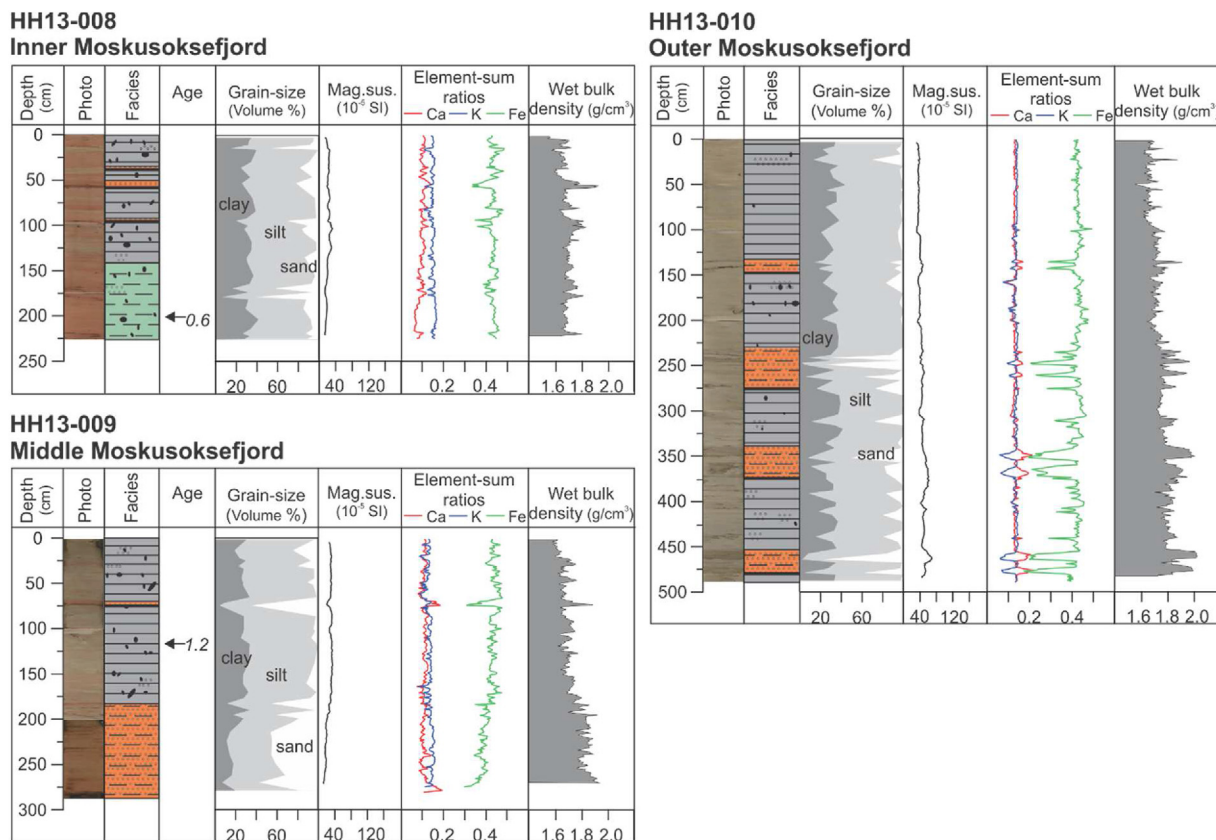


Fig. 10. Composite logs of core HH13-008, HH13-009 and HH13-010 retrieved from Moskusoksefjord, showing lithofacies, line-scan images, grain-size distribution, physical properties and XRF core-scanning geochemistry. The latter presents the ratio of selected elements over the eight most abundant elements. See Fig. 8 for legend to the lithofacies. Calibrated radiocarbon ages, presented in calibrated years before present, are indicated with arrows. Core locations are shown on Fig. 1.

Table 5
Linear sedimentation rates for the sampled glacial marine intervals. (*from Evans et al. (2002)).

Core	Depth (cm)	Age interval (ka cal BP)	Sedimentation rate (cm/ka)
HH13-008	0–202	0–0.6	331
HH13-009	0–117	0–1.2	98
HH13-011	0–592	0–1.1	519
HH13-012	0–195	0–0.7	281
	195–454	0.7–7.8	37
PS2633	64–206	7.9–8.75	170
PS2632	0–8	0–0.52	15
	8–97	0.52–1.1	157
PS2631	0–99	0–1.1	91*
	99–390	1.1–8.3	40*
	390–573	8.3–10.8	72
	573–707	10.8–11.2	408

Two radiocarbon ages of 1.1 ka cal BP and 0.52 ka cal BP from the upper half of core PS2632 give an estimated linear sedimentation rate in middle Kejsjer Franz Josef Fjord of 157 cm/ka for this time interval (Table 3), almost twice the rate in the outermost fjord (PS2631) in the same interval (for core locations, see Fig. 1c). In inner Kejsjer Franz Josef Fjord (PS2633), the lithofacies containing laminated mud was deposited prior to 8.75 ka cal BP, whilst the overlying massive mud was deposited between 8.75 and 7.9 ka cal BP. The estimated linear sedimentation rate for the inner fjord is 170 cm/ka between 8.75 and 7.9 ka cal BP.

4.5. Chronology and sediment rates

A total of 14 new radiocarbon ages were retrieved in this study; nine from Kejsjer Franz Josef Fjord, three from Nordfjord and two from Moskusoksefjord (Figs. 8–10; Table 2). The two radiocarbon

ages in the laminated lithofacies at the base of core PS2631 give a minimum age range of 11.2–10.8 ka cal BP. The overlying massive mud with dispersed clasts yielded ages of 8.3 and 1.1 ka cal BP. Thus, the estimated linear sedimentation rate can be further constrained; in outer Kejsjer Franz Josef Fjord it was very high between 11.2 and 10.8 ka cal BP (408 cm/ka). Then it dropped markedly to 72 cm/ka between 10.8 and 8.3 ka cal BP, reduced further to 40 cm/ka from 8.3–1.2 ka cal BP before doubling to 91 cm/ka from 1.2 ka cal BP to present (Table 3).

In Nordfjord, radiocarbon dates from the bases of HH13-011 and HH13-012 yielded ages of 1.1 ka cal BP and 7.8 ka cal BP, respectively (Fig. 9; Table 2). An additional sample from core HH13-012 at 195 cm depth provided an age of 0.7 ka cal BP. Assuming a linear sedimentation rate, the minimum average sedimentation rate for core HH13-011 is 519 cm/ka. At the site of core HH13-012, it is estimated to be 37 cm/ka between 7.8 and 0.7 cal yrs BP and 281 cm/ka between 0.7 ka cal BP and the present (Table 3).

A sample collected within the massive mud in core HH13-008 from Moskusoksefjord provided an age of 0.6 ka cal BP, while a sample within the laminations in core HH13-009 provided an age of 1.2 ka cal BP (Fig. 10). Sedimentation rates of minimum 331 cm/ka and 98 cm/ka have been estimated for inner and middle Moskusoksefjord, respectively (Table 3).

In summary, the sedimentation rates between ~11.2–8.3 ka cal BP in Kejsjer Franz Josef Fjord dramatically dropped from 408 cm/ka to 72 cm/ka. The period between ~8.3–1.0 ka cal BP is characterized by low sedimentation rates in both Nordfjord and Kejsjer Franz Josef

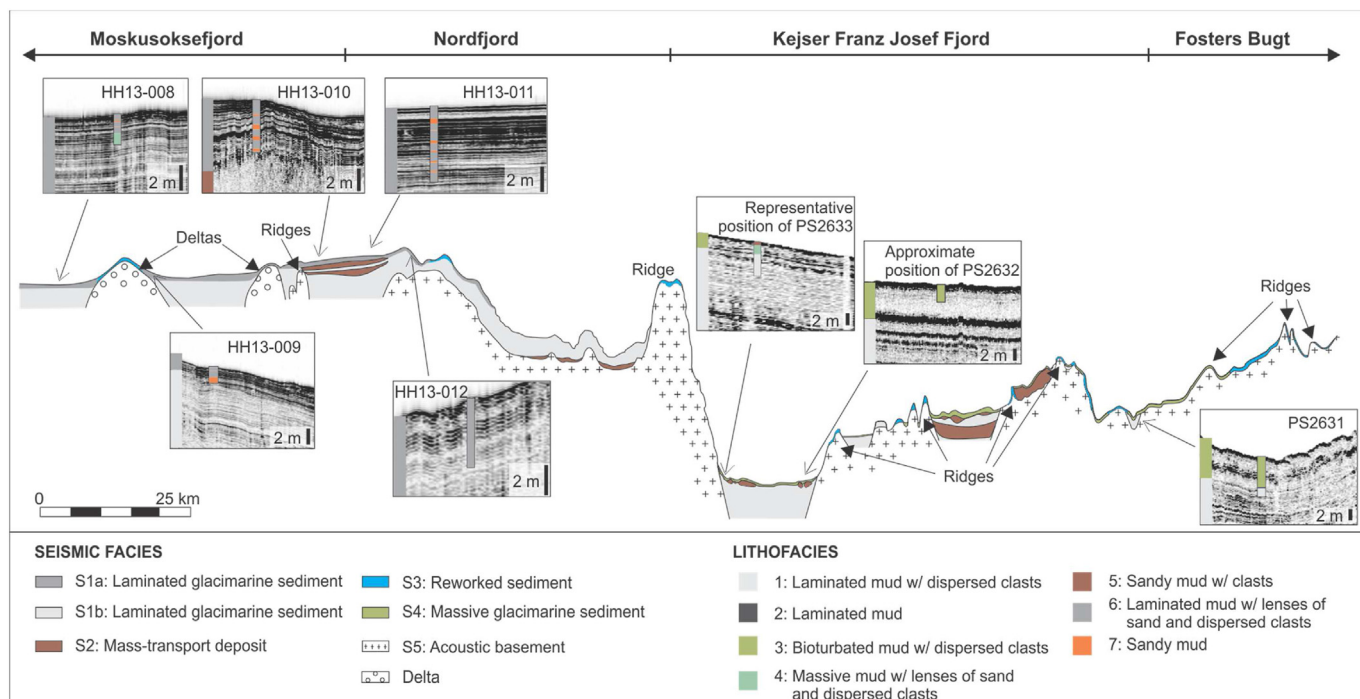


Fig. 11. Conceptual model of the interpreted seismostratigraphic facies and their distribution within Moskusoksefjord, Nordfjord and Kejser Franz Josef Fjord. Note that the landforms and thickness of individual seismic facies are not to scale. The locations and approximate penetration depth of the gravity cores are shown. For location of the bathymetric profile, see Fig. 3.

Fjord (~40 cm/ka), whereas the last ~1.0 ka cal BP is characterized by low to medium rates (15–157 cm/ka) in Kejser Franz Josef Fjord, and high rates in Nordfjord and Moskusoksefjord (98–519 cm/ka).

5. Discussion

5.1. Deglacial events in the Kejser Franz Josef Fjord system

The assemblage of ridges within our study area is interpreted to reflect the position of the grounding line as the ice stream retreated through the Kejser Franz Josef Fjord system during the deglaciation following the Last Glacial Maximum (Fig. 6c, d, e, f and 11). The dynamics and drivers of this stepwise ice retreat can be explained from the dimensions, positions, and age estimates of these moraine ridges.

The moraines within Fosters Bugt indicate that overall ice front retreat was punctuated by up to five readvances or stillstands (Fig. 6d and f). A generally thin sediment drape (seismic facies S3 and S4), interpreted to be deposited by meltwater, overlies the acoustic impenetrable facies 5 interpreted as subglacial till and/or bedrock (Fig. 11). The thin drape may indicate a low meltwater production and hence low sediment production during the early deglaciation. A rapid global sea-level rise of ~20 m in 1500 years has been identified in the period from ~14 to 12.5 ka BP (Lambeck et al., 2014), which could explain the ice retreat in this period.

The morphology of Kejser Franz Josef Fjord is dominated by moraines and local sedimentary depocenters of glacimarine sediments (Figs. 6c and 11). The locations of moraines close to the fjord mouth and in connection to fjord narrowing and shallowing indicate that local changes in fjord geometry provided pinning points (Figs. 3 and 11) for the retreating ice front, causing it to stabilize and possibly readvance. This suggests that the fjord geometry had a locally varying impact on the deglaciation dynamics of Kejser Franz Josef Fjord. The accumulations of glacimarine sediments (facies

S1b) are largely concentrated in front of moraines. We attribute this to underflows, implying melting of the glacier as the front stabilized at pinning points.

As the ice margin reached the retrograde slope in Kejser Franz Josef Fjord (Fig. 3), the ice mass transport from the catchment area within the GrIS continued to deliver enough ice to keep the glacier grounded. An additional explanation for the repeated stabilization on a retrograde slope may be ice-shelf buttressing, contributing to grounding line stabilization (cf. Gudmundsson, 2013). Prominent moraine ridges at the fjord mouths of Nordfjord, Geologifjord and the innermost Kejser Franz Josef Fjord (Eleonores Bugt) indicate longer stillstands of the ice margin. This was likely facilitated by the change in fjord morphology in these areas, which acted as bottlenecks with increased ice flux, promoting ice front stabilization (cf. Åkesson et al., 2018).

Glacial landforms are absent on the seafloor in Moskusoksefjord, apart from two partly transverse ridges in the outer basin of Moskusoksefjord (Figs. 3, 4 and 11). These ridges are surrounded by basins overlain by a draping unit of glacimarine sediments (facies S1) that can be followed throughout Nordfjord and Moskusoksefjord. The preservation of onshore landforms as raised delta terraces indicate that Moskusoksefjord was deglaciated after the formation of the ridges. As such, these ridges may be moraines formed during the deglaciation of Moskusoksefjord.

Two levels of up to 40 m thick lobe-shaped deposits (seismic facies S2) consisting of sandy mud are identified on the sub-bottom profiles from outer Moskusoksefjord and inner Nordfjord (Figs. 6 and 11). The lobe-shaped deposits, located beyond the moraine mapped closest to the present-day front of Waltershausen Gletscher, indicate at least two readvances of the glacier front followed by redistribution of sediments from moraine ridges. Similar lobe shaped sediment deposits are also identified in other parts of the Kejser Franz Josef Fjord system (Fig. 11), as well as in Arctic fjords (c.f. Plassen et al. (2004) and references therein).

5.2. Deglaciation chronology

The integration of our new marine data with existing results provides the opportunity to establish an improved deglaciation history of Fosters Bugt, Kejser Franz Josef Fjord, Nordfjord and Moskusoksefjord (Fig. 12). This reconstruction includes recalibration of previously published radiocarbon dates (Table 2).

Recalibrated radiocarbon ages from the mid-shelf (core PS2630; Evans et al., 2002) and outer Kejser Franz Josef Fjord (core PS2631; Andrews et al., 2016) show that the mid-shelf grounding zone wedge and outer fjord moraines were formed between ~15.5 and 11.2 ka cal BP (Fig. 12b and c) as the onset of glacial-marine sedimentation occurred at this time on mid-shelf and in Fosters Bugt, respectively, indicating that they are Bølling/Allerød and Younger Dryas-Preboreal in age (Fig. 12b and c).

The position of the outermost moraine in Fosters Bugt complements the moraine belt mapped by Hjort (1979) on eastern Hold With Hope and Geographical Society Ø, supporting a postulated maximum position of the ice margin during the Younger Dryas-early Preboreal here (Fig. 12c), as also suggested by Evans et al. (2002). An alternative maximum ice extent was proposed by Arndt (2018), inferring that the ice stream readvanced from the fjord entrance to a mid-shelf position during the Younger Dryas. If correct, the ice stream readvanced more than 100 km to a the mid-shelf position. Also, further south in East Greenland, two events of glacial advance during Younger Dryas-Preboreal time are located onshore: the eastern Jameson Land moraines and Milne Land

moraine belt in the Scoresby Sund area (e.g. Funder, 1978; Alexanderson and Håkansson, 2014). We therefore find it less likely that the ice front re-advanced to a mid-shelf position within our study area, and, based on our data and previously published onshore data, we favor the interpretation of a maximum ice front position in Fosters Bugt during the Younger Dryas-Preboreal period.

The minimum deglaciation age of 11.2 ka cal BP in outer Kejser Franz Josef Fjord is in line with the onshore deglaciation of both western Gauss Halvø and Geographical Society Ø, with minimum deglaciation ages of 9.8 and 10.9 ka cal BP, respectively (Weidick, 1977; Wagner et al., 2010) (Fig. 12a). The radiocarbon ages obtained within the ice-proximal sediment facies imply that the glacier margin was located nearby for minimum 400 years before retreating further in-fjord after 10.8 ka cal BP. If synchronous, the stillstands at the fjord mouth of Nordfjord, Geologifjord and Eleonores Bugt are interpreted to have lasted until ~8.75 ka cal BP, marked by a change in facies from laminated mud to massive mud in core PS2633, suggesting a transition from an ice-proximal to an ice-distal setting. Thus, the minimum age for the formation of the recessional moraines in Kejser Franz Josef Fjord are between 11.2 and 8.75 ka cal BP, i.e. during the Early Holocene (the Greenlandian Stage), the HTM period characterized by climate oscillations and a generally rising temperature to higher air temperatures than today (Rasmussen et al., 2007; Walker et al., 2018), marginal sea-ice coverage and enhanced inflow of warm Atlantic waters on the East Greenland shelf (Koç et al., 1993; Müller et al., 2012).

Whereas the deglaciation of inner Kejser Franz Josef Fjord and

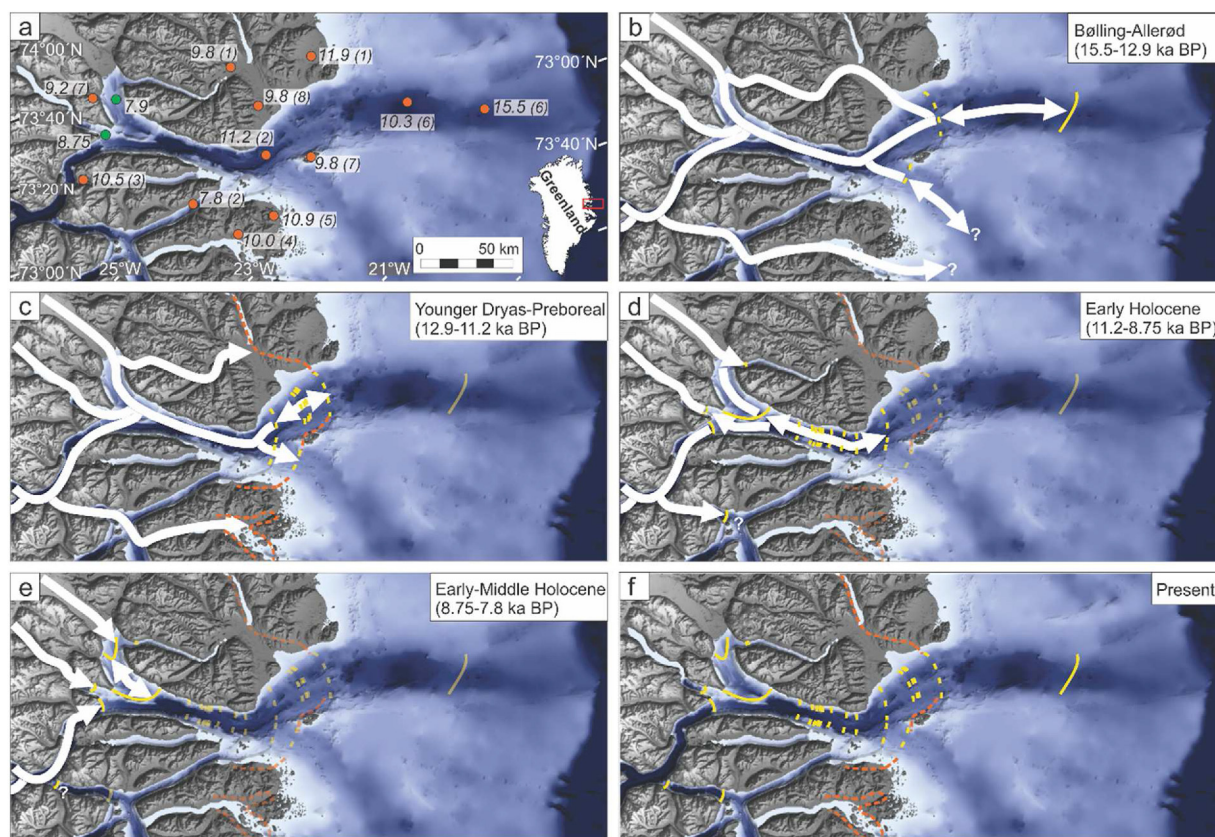


Fig. 12. Reconstruction of the ice sheet extent and dynamics in the Kejser Franz Josef Fjord system from the Bølling-Allerød to present. Solid white arrows indicate ice flow directions. The location of mapped grounding-zone wedges and recessional moraines are indicated with yellow lines. The first panel includes green circles showing our new minimum deglaciation ages, while orange circles show the locations of existing deglaciation radiocarbon ages. All ages are presented in calibrated years before present (ka cal BP). 1: Håkansson (1975); 2: Andrews et al. (2016); 3: Wagner and Melles (2002); 4: Wagner et al. (2000); 5: Wagner et al. (2010); 6: Evans et al. (2002); 7: Weidick (1976); 8: Weidick (1977). For details about the radiocarbon ages, see Table 2. (Bathymetry and topography from IBCAO v.4.0; Jakobsson et al., 2020). (For interpretation of the references to color in this figure legend, the reader is referred to the Web version of this article.)

Nordfjord occurred prior to 8.75 ka cal BP and 7.8 ka cal BP, respectively (Fig. 12d and e), lake records on Ymer Ø in inner Kejser Franz Josef Fjord imply that the deglaciation of the island commenced earlier, prior to 10.5 ka cal BP (Wagner and Melles, 2002), whereas eastern Strindberg Land west of Nordfjord was deglaciated prior to 9.2 ka cal BP (Weidick, 1976). A possible explanation for this apparent offset in the deglaciation of the fjords relative to the surrounding land area is that ice retreat was accompanied with ice sheet thinning, confining the ice margin fluctuations to the fjord basin while the surrounding land areas were more or less ice-free.

The sediment cores located closest to the present-day glacier front of Waltershausen Gletscher (10–14 km (HH13-010, HH13-011 and HH13-012); Fig. 1c) show no changing trends in sediment grain-size, geochemistry or physical properties (Figs. 9 and 10). Based on this, we find no signs of any major glacier front readvances over the core sites during the last 7.8 ka cal BP. Nevertheless, the increase in sedimentation rate from 700 years BP and present (281 cm/ka), relative to from 7.8 to 0.7 ka cal BP (37 cm/ka), indicates that the meltwater supply in Nordfjord increased towards the Late Holocene. A possible explanation for this is that an early Holocene Thermal Maximum warming (Wagner et al., 2000, 2010; Wagner and Melles, 2002) led Waltershausen Gletscher to retreat further inland, followed by a subsequent cooling and readvance during the Little Ice Age. However, the presence of IRD throughout core 012 in outer Nordfjord (Fig. 9; see also Evans et al. (2002)) is interpreted to show that the Waltershausen Gletscher remained marine-terminating during the last 7.8 ka cal BP. This continuous delivery of iceberg debris to the core site suggest that the glacier was relatively stable, even when subjected to the Holocene Thermal Maximum warming. An alternative interpretation involves increased input from nearby icecaps (Fig. 1b) which may have grown during the Little Ice Age. Further studies are needed to better clarify this.

5.3. Ice margin retreat rates

We calculate a minimum average retreat rate of 96 m a^{-1} between the outermost moraine in Fosters Bugt and the fjord mouth of Kejser Franz Josef Fjord, given that the ice stream remained stationary at its maximum position until the end of the Younger Dryas. This rate is within the range of ice margin retreat across Store Koldewey Trough, offshore NE Greenland ($80\text{--}400 \text{ m a}^{-1}$; Olsen et al., 2020) and offshore NW Greenland ($22\text{--}275 \text{ m a}^{-1}$; Newton et al., 2017; Ó Cofaigh et al., 2013). However, the minimum retreat rate does not account for the five stillstand events across Fosters Bugt. Thus, improved chronologies remain required to provide more precise estimates of the retreat across Fosters Bugt during the last deglaciation.

Assuming that the ice front retreated at a steady rate through Kejser Franz Josef Fjord and Nordfjord during the Early and Middle Holocene (Fig. 12), the minimum average retreat rate in this period were 35 m a^{-1} and 33 m a^{-1} , respectively. These rates are within estimates of ice-front retreat of $10\text{--}80 \text{ m a}^{-1}$ in southeast Greenland fjords, e.g. Kangerdlugssuaq Fjord, Sermilik Fjord and Bernstorffs Fjord (Andrews et al., 1994; Hughes et al., 2012; Dyke et al., 2014). Whereas the southeast GrIS is inferred to have undergone relatively rapid and continuous retreat through the fjord systems, Kejser Franz Josef Fjord encompasses geomorphological evidence of an episodic retreat. The sets of recessional moraines imply that the ice stream occupying the Kejser Franz Josef Fjord system underwent a stepwise retreat characterized by several

stillstands and/or readvances of the grounding line during the last deglaciation.

For the Fennoscandian Ice Sheet, average retreat rates from the Andfjorden – Vågsfjorden system (excluding the shelf trough part) in northern Norway has been estimated to $31\text{--}67 \text{ m a}^{-1}$ (Vorren and Plassen, 2002), i.e. relatively similar to the rates reported here. This leads us to suggest the same overall control for the deglaciation of the part of both these ice sheets overlying an alpine coastal landscape, ice melting from increased Northern Hemisphere summer insolation that peaked in Early Holocene.

5.4. Deglacial infilling of a NE Greenland fjord: sediment sources and sedimentation rates

Sampling of the upper part of the stratigraphy reveal a lithological sequence starting with laminated mud (lithofacies 1; facies S1b) and a relatively high sedimentation rate, overlain by bioturbated mud (lithofacies 3; facies S4) (Fig. 11) with a marked drop in sedimentation rate (Table 3). Together with the sediment distribution, with increased accumulations of glacial marine sediments in front of moraines, we interpret the sediments to include the transition from an ice-proximal to an ice-distal environment as the ice front retreated through the Kejser Franz Josef Fjord system.

The dominance of glacial marine laminated mud (Figs. 8–10), together with sedimentary basin infill (Fig. 6a and b and 11) in the Kejser Franz Josef Fjord system, demonstrate that suspension settling of fine-grained sediments from sediment-laden glacial meltwater plumes acted as the primary depositional process (Fig. 13). Other studies of glacial marine processes in Greenland fjords show that suspension settling act as the key sedimentary process, emphasizing the importance of meltwater-related processes in ice-proximal areas of GrIS outlet glaciers (e.g. Smith and Andrews, 2000; Ó Cofaigh et al., 2001; Streuff et al., 2017). This dominant role of meltwater from Waltershausen Gletscher to the sedimentary environment may be explained by i) increased melting of the ice margin due to ice-ocean interactions and/or ii) increased ice sheet surface melt, as seen on the present surface of the GrIS (Noël et al., 2019). Dispersed clasts and lenses of sand are observed sporadically, with generally increasing amounts with increasing distance from glacier margins, and this is related to density currents (Figs. 11 and 13). Whereas the layers of sandy mud in outer Moskusoksefjord and inner Nordfjord are attributed to density currents from Waltershausen Gletscher, the sandy mud in inner and middle Moskusoksefjord are interpreted to be related to fluvial processes from the nearby deltas creating local depocenters (topographic highs) influencing sediment distribution within the fjord.

The repeatedly changing sediment color within the laminated mud in Moskusoksefjord (Fig. 10) demonstrates input from multiple source areas (cf. Forwick and Vorren, 2009): the red sediments are delivered from the Old Red Sandstone surrounding Moskusoksefjord (Figs. 2 and 10), while the gray sediments dominate in the proximity to Waltershausen Gletscher (Figs. 8 and 9). The pinkish gray sediments probably represent a mixture of the two. Thus, based on the reddish sediment color in the middle- and inner basins of Moskusoksefjord, we interpret the stratified acoustic signature in Moskusoksefjord to be highly influenced by local hemipelagic sedimentation and re-sedimentation along the steep fjord slopes (Fig. 13).

Despite of reflecting similar sedimentary processes, the deposits in the study area reveal differences in physical properties and geochemical compositions. The magnetic susceptibility and Ca/sum ratios generally decrease in Nordfjord and Moskusoksefjord with

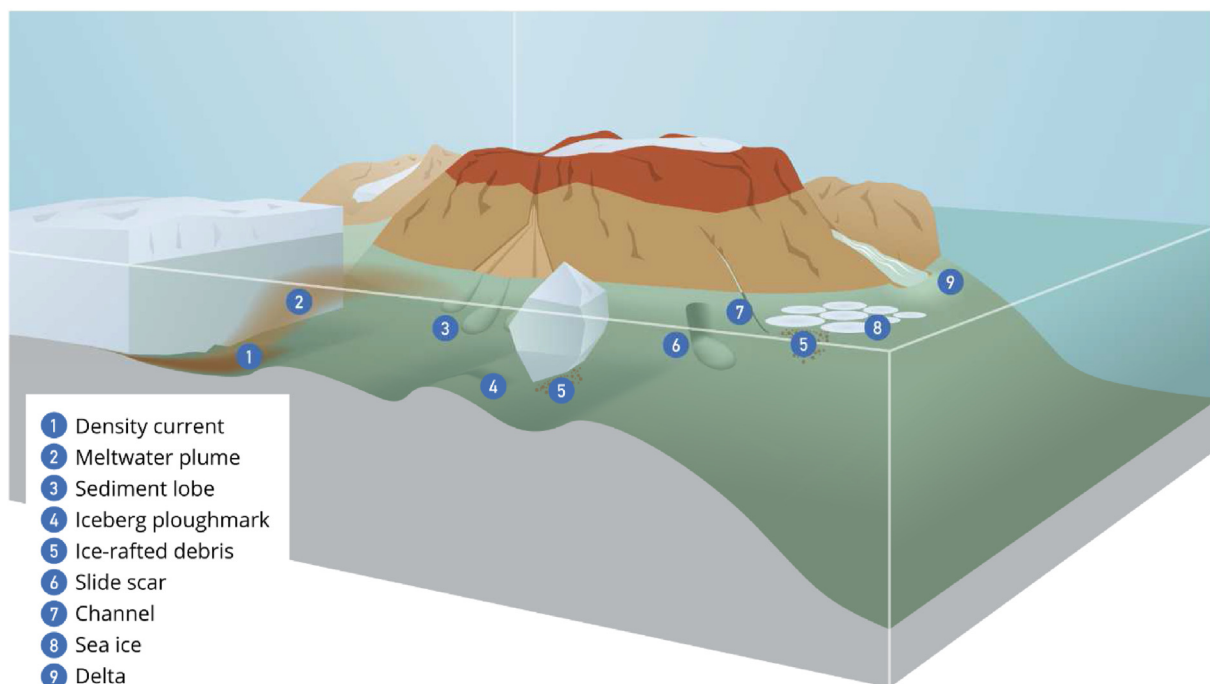


Fig. 13. Conceptual sketch of the different sedimentary processes in Moskusoksefjord.

increasing distance to Waltershausen Gletscher (Figs. 9 and 10). This suggests that the highest susceptibility values and calcium concentrations are derived from the glacially eroded Neoproterozoic to Ordovician Caledonian fold belts in the glacier catchment area, compared to the Devonian continental siliciclastic sediments surrounding Moskusoksefjord (Fig. 2). In outer Keiser Franz Josef Fjord, larger variations in the geochemistry and magnetic susceptibility values indicate that sediment deposition was influenced by a larger drainage area (Fig. 8), including local sediment sources as well as by sediments transported within the East Greenland Current.

The estimated average sedimentation rates in outer Keiser Franz Josef Fjord and inner Nordfjord ranged from 91 to 519 cm/ka during the last ~1 ka and 47–58 cm/ka during the last ~8 ka (Table 3). They are comparable to the estimated sedimentation rates of 110–340 cm/ka during the last ~1 ka in southeastern Greenland fjords (Nansen Fjord, Mikis Fjord and Kangerdlugssuaq Fjord; Andrews et al., 1994). Variations in sediment thickness on the sub-bottom profiles reveal that the sediment distribution in the study area depends on multiple factors including the distance to large sediment sources, e.g. Waltershausen Gletscher and the river at the fjord head of Moskusoksefjord, as well as the topography with a typically thicker sediment package in basins (Figs. 6 and 11) (cf. Syvitski, 2003). In Nordfjord, we attribute the drop in sedimentation rates from approximately 519 cm/ka during the last 1.1 ka cal BP to approximately 281 cm/ka during the last 0.69 ka cal BP, to an elevation separating the two sub-basins creating an obstacle for sediment transport along the seafloor (Fig. 6b). The apparent low average sedimentation rate during the last 7.9 ka cal BP in inner Keiser Franz Josef Fjord, together with the lower erosional boundary and abrupt increase in wet bulk density (Fig. 8), is speculated to be a result of mass-wasting and erosion of the sediments.

6. Conclusions

Investigations of new and previously published marine acoustic data (swath bathymetry and high-resolution seismic profiles),

supplemented with multi-proxy analyses of sediment cores, provide new information on the Late Weichselian and Holocene glacial history and the paleoenvironmental development in a 190 km long shelf-fjord transect in the Fosters Bugt-Keiser Franz Josef Fjord system, NE Greenland.

- A complex of moraines located in Fosters Bugt, together with radiocarbon ages, supports the theory of a maximum ice front position near the fjord entrance during the Younger Dryas-Preboreal period.
- The outer and inner Keiser Franz Josef Fjord was deglaciated prior to 11.2 and 8.75 ka cal BP. Nordfjord was deglaciated by 7.8 ka cal BP.
- The apparent delay in the deglaciation of the fjord basins relative to the surrounding land areas suggest that the local ice retreat in the study area was accompanied with thinning of this part of the GrIS, confining the ice margin fluctuations to the fjords.
- The retreat moraines within the fjord system provide evidence of a stepwise retreat during the deglaciation, interrupted by episodes of stillstands and/or readvances of the grounding line. Paleo-ice stream retreat rates are estimated to have ranged between 33 and 96 m a⁻¹.
- The sediment supply from Waltershausen Gletscher dominated Keiser Franz Josef Fjord, Nordfjord and outer Moskusoksefjord throughout the Holocene period, whereas in the middle and inner Moskusoksefjord the sediment deposits reflect the local catchment area. The estimated average sedimentation rates ranged from 91 to 519 cm/ka during the last ~1 ka and 47–58 cm/ka during the last ~8 ka.

Declaration of competing interest

The authors declare that they have no known competing financial interests or personal relationships that could have appeared to influence the work reported in this paper.

Acknowledgements

We would like to thank the captains, crew and participants onboard the 2013 cruise with *R/V Helmer Hanssen*, arranged by the TUNU program, and the ARK X cruise in 1994 with *R/V Polarstern*. Further, we acknowledge the technical staff and laboratory engineers at UiT The Arctic University of Norway and AWI Bremerhaven during and after the cruises. Special thanks go to Jens Matthiessen, Jutta Wollenburg and Catalina Gebhardt at AWI for helping with data collection and management. Data from the ARK X cruise are available through the information system PANGAEA (<https://www.pangaea.de/>). Finally, we would like to thank Editor Colm Ó Cofaigh and our two referees, including Jeff Evans, for their thorough and constructive reviews, as well as thoughtful comments that improved the manuscript.

References

- Åkesson, H., Nisancioglu, K.H., Nick, F.M., 2018. Impact of fjord geometry on grounding line stability. *Front. Earth Sci.* 6, 1–16. <https://doi.org/10.3389/feart.2018.00071>.
- Alexanderson, H., Håkansson, L., 2014. Coastal glaciers advanced onto Jameson Land, East Greenland during the late glacial-early Holocene Milne Land Stade. *Polar Res.* 33. <https://doi.org/10.3402/polar.v33.20313>.
- An, L., Rignot, E., Wood, M., Willis, J.K., Mouginit, J., Khan, S.A., 2021. Ocean melting of the Zachariae Isstrøm and Nioghalvfjærdsfjorden glaciers, northeast Greenland. *P Natl Acad Sci USA* 118. <https://doi.org/10.1073/pnas.2015483118>.
- Andresen, A., Rehnström, E.F., Holte, M., 2007. Evidence for simultaneous contraction and extension at different crustal levels during the Caledonian orogeny in NE Greenland. *J. Geol. Soc. London* 164, 869. <https://doi.org/10.1144/0016-76492005-056>. LP – 880.
- Andrews, J.T., Milliman, J.D., Jennings, A.E., Rynes, N., Dwyer, J., 1994. Sediment thicknesses and Holocene glacial marine sedimentation rates in three east Greenland fjords (ca.68°N). *J. Geol.* 102, 669–683.
- Andrews, J.T., Smith, L.M., Preston, R., Cooper, T., Jennings, A.E., 1997. Spatial and temporal patterns of iceberg rafting (IRD) along the East Greenland margin, ca. 68°N, over the last 14 cal.ka. *J. Quat. Sci.* 12, 1–13. [https://doi.org/10.1002/\(SICI\)1099-1417\(199701/02\)12:1<1::AID-JQS288>3.0.CO;2](https://doi.org/10.1002/(SICI)1099-1417(199701/02)12:1<1::AID-JQS288>3.0.CO;2).
- Andrews, J.T., Stein, R., Moros, M., Perner, K., 2016. Late Quaternary changes in sediment composition on the NE Greenland margin (~73° N) with a focus on the fjords and shelf. *Boreas* 45, 381–397. <https://doi.org/10.1111/bor.12169>.
- Arndt, J.E., 2018. Marine geomorphological record of ice sheet development in East Greenland since the last glacial maximum. *J. Quat. Sci.* 33, 853–864. <https://doi.org/10.1002/jqs.3065>.
- Arndt, J.E., Jokat, W., Dorschel, B., 2017. The last glaciation and deglaciation of the Northeast Greenland continental shelf revealed by hydro-acoustic data. *Quat. Sci. Rev.* 160, 45–56. <https://doi.org/10.1016/j.quascirev.2017.01.018>.
- Arndt, J.E., Jokat, W., Dorschel, B., Myklebust, R., Dowdeswell, J.A., Evans, J., 2015. A new bathymetry of the Northeast Greenland continental shelf: constraints on glacial and other processes. *G-cubed* 16, 3733–3753. <https://doi.org/10.1002/2015GC005931>.
- Batchelor, C.L., Dowdeswell, J.A., Rignot, E., 2018. Submarine landforms reveal varying rates and styles of deglaciation in North-West Greenland fjords. *Mar. Geol.* 402, 60–80. <https://doi.org/10.1016/j.margeo.2017.08.003>.
- Batchelor, C.L., Dowdeswell, J.A., Rignot, E., Millan, R., 2019. Submarine moraines in southeast Greenland fjords reveal contrasting outlet-glacier behavior since the last glacial maximum. *Geophys. Res. Lett.* 46, 3279–3286. <https://doi.org/10.1029/2019GL082556>.
- Bellwald, B., Hjelstuen, B.O., Sejrup, H.P., Stokowy, T., Kuvås, J., 2019. Holocene mass movements in west and mid-Norwegian fjords and lakes. *Mar. Geol.* 407, 192–212. <https://doi.org/10.1016/j.margeo.2018.11.007>.
- Bøe, R., Hovland, M., Instanes, A., Rise, L., Vasshus, S., 2000. Submarine slide scars and mass movements in Karmsundet and Skudenesfjorden, southwestern Norway: morphology and evolution. *Mar. Geol.* 167, 147–165.
- Bogen, J., 1983. Morphology and sedimentology of deltas in fjord and fjord valley lakes. *Sediment. Geol.* 36, 245–267.
- Boulton, G.S., 1990. Sedimentary and sea level changes during glacial cycles and their control on glacial marine facies architecture. In: Dowdeswell, J.A., Scourse, J.D. (Eds.), *Glacimarine Environments: Processes and Sediments*. Geological Society Special Publications, pp. 15–52.
- Box, J.E., 2002. Survey of Greenland instrumental temperature records: 1873–2001. *Int. J. Climatol.* 22, 1829–1847. <https://doi.org/10.1002/joc.852>.
- Catania, G.A., Stearns, L.A., Moon, T.A., Enderlin, E.M., Jackson, R., 2019. Future evolution of Greenland's marine-terminating outlet glaciers. *J. Geophys. Res-Earth* 1–28. <https://doi.org/10.1029/2018jfo04873>.
- Christiansen, J.S., 2012. The TUNU-programme: euro-arctic marine fishes – diversity and adaption. In: Di Prisco, G.V.C. (Ed.), *Adaptation and Evolution in Marine Environments*, vol. 1. Springer, Berlin, Heidelberg, pp. 35–50. https://doi.org/10.1007/978-3-642-27352-0_3. From Pole to Pole.
- Copernicus Sentinel Data, 2020, 3.11.20.
- Corner, G.D., 2006. A transgressive–recessive model of fjord-valley fill: stratigraphy, facies and depositional controls. In: Dalrymple, R.W., Leckie, D.A., Tillman, R.W. (Eds.), *Incised Valleys in Time and Space*. SEPM Special Publication, pp. 161–178.
- Dijkstra, N., Junntila, J., Skirbekk, K., Carroll, J.L., Husum, K., Hald, M., 2017. Benthic foraminifera as bio-indicators of chemical and physical stressors in Hammerfest harbor (Northern Norway). *Mar. Pollut. Bull.* 114, 384–396. <https://doi.org/10.1016/j.marpolbul.2016.09.053>.
- Dowdeswell, J.A., Uenzelmann-Neben, G., Whittington, R.J., Marienfeld, P., 1994. The late quaternary sedimentary record in Scoresby Sund, east Greenland. *Boreas* 23, 294–310. <https://doi.org/10.1111/j.1502-3885.1994.tb00602.x>.
- Dyke, L.M., Hughes, A.L.C., Murray, T., Hiemstra, J.F., Andresen, C.S., Rodés, A., 2014. Evidence for the asynchronous retreat of large outlet glaciers in southeast Greenland at the end of the last glaciation. *Quat. Sci. Rev.* 99, 244–259. <https://doi.org/10.1016/j.quascirev.2014.06.001>.
- Evans, J., Dowdeswell, J.A., Grobe, H., Niessen, F., Stein, R., Hubberten, H.-W., Whittington, R.J., 2002. Late quaternary sedimentation in Keiser Franz Joseph Fjord and the continental margin of east Greenland. *Geol. Soc. Spec. Publ.* 203, 149–179. <https://doi.org/10.1144/GSL.SP.2002.203.01.09>.
- Evans, J., Ó Cofaigh, C., Dowdeswell, J.A., Wadhams, P., 2009. Marine geophysical evidence for former expansion and flow of the Greenland Ice Sheet across the north-east Greenland continental shelf. *J. Quat. Sci.* 24 (3), 279–293. <https://doi.org/10.1002/jqs.1231>.
- Forwick, M., Husum, K., Laberg, J.S., Dahl, T.M., Olsen, B.R., 2013. Marine-geological Work during the TUNU-V Expedition to East Greenland Fjords and the East Greenland Continental Margin on *R/V Helmer Hanssen*. August 5th – 17th 2013 (Tromsø).
- Forwick, M., Vorren, T.O., 2009. Late Weichselian and Holocene sedimentary environments and ice rafting in Isfjorden, Spitsbergen. *Palaeogeogr. Palaeoclimatol.* 280, 258–274. <https://doi.org/10.1016/j.palaeo.2009.06.026>.
- Forwick, M., Vorren, T.O., 2010. Stratigraphy and deglaciation of the Isfjorden area, Spitsbergen. *Norw. J. Geol.* 90, 163–179.
- Forwick, M., Vorren, T.O., 2012. Submarine mass wasting in Isfjorden, Spitsbergen. In: Yamada, Y., Kawamura, K., Ikehara, K., Ogawa, Y., Urgeles, R., Mosher, D., Chaytor, J., Strasser, M. (Eds.), *Submarine Mass Movements and Their Consequences*. Springer Netherlands, Dordrecht, pp. 711–722.
- Funder, S., 1970. Notes on the glacial geology of eastern Milne Land. *Rapp. - Grnl. Geol. Undersøgelse* 30, 37–42.
- Funder, S., 1978. Holocene stratigraphy and vegetation history in the Scoresby Sund area, East Greenland. *Grønland. Geol. Unders.* 129, 1–76.
- Funder, S., Kjeldsen, K.K., Kjær, K.H., Ó Cofaigh, C., 2011. The Greenland ice sheet during the past 300,000 Years: a review. *Dev. Quat. Sci.* 15, 699–713. <https://doi.org/10.1016/B978-0-444-53447-7.00050-7>.
- Gales, J.A., Talling, P.J., Cartigny, M.J.B., Clarke, J.H., Lintern, G., Stacey, C., Clare, M.A., 2019. What controls submarine channel development and the morphology of deltas entering deep-water fjords? *Earth. Surf. Proc. Land.* 44, 535–551. <https://doi.org/10.1002/esp.4515>.
- Gjelstrup, C.V.B., 2021. Hydrographic Changes of Northeast Greenland Fjords and Coast. Technical University of Denmark.
- Grant, J.A., Schreiber, R., 1990. Modern swathe sounding and sub-bottom profiling technology for research applications: the Atlas Hydrosweep and Parasound Systems. *Mar. Geophys. Res.* 12, 9–19. <https://doi.org/10.1007/BF00310559>.
- Gudmundsson, G.H., 2013. Ice-shelf buttressing and the stability of marine ice sheets. *Cryosphere* 7, 647–655. <https://doi.org/10.5194/tc-7-647-2013>.
- Håkansson, S., 1975. University of Lund radiocarbon dates VIII. *Radiocarbon* 17, 174–195. <https://doi.org/10.1017/S0033822200002034>.
- Heaton, T.J., Köhler, P., Butzin, M., Bard, E., Reimer, R.W., Austin, W.E.N., Ramsey, C.B., Grootes, P.M., Hughen, K.A., Kromer, B., Reimer, P.J., Adkins, J., Burke, A., Cook, M.S., Olsen, J., Skinner, L.C., 2020. Marine20 – the marine radiocarbon age calibration curve (0–55,000 cal BP). *Radiocarbon* 62, 779–820. <https://doi.org/10.1017/RDC.2020.68>.
- Higgins, A.K., Elvevold, S., Escher, J.C., Frederiksen, K.S., Gilotti, J.A., Henriksen, N., Jepsen, H.F., Jones, K.A., Kalsbeek, F., Kinny, P.D., Leslie, A.G., Smith, M.P., Thrane, K., Watt, G.R., 2004. The foreland-propagating thrust architecture of the East Greenland Caledonides 72°–75°N. *J. Geol. Soc. London* 161, 1009. <https://doi.org/10.1144/0016-764903-141>. LP – 1026.
- Hjelstuen, B.O., Hafliðason, H., Sejrup, H.P., Lyså, A., 2009. Sedimentary processes and depositional environments in glaciated fjord systems – evidence from Nordfjord, Norway. *Mar. Geol.* 258, 88–99. <https://doi.org/10.1016/j.margeo.2008.11.010>.
- Hjort, C., 1979. Glaciation in northern east Greenland during the late Weichselian and early Flandrian. *Boreas* 8, 281–296.
- Hogan, K.A., Colm, O., Jennings, A.E., Dowdeswell, J.A., Hiemstra, J.F., 2016. Deglaciation of a major palaeo-ice stream in Disko Trough, west Greenland. *Quat. Sci. Rev.* 147, 5–26. <https://doi.org/10.1016/j.quascirev.2016.01.018>.
- Hogan, K.A., Jakobsson, M., Mayer, L., Reilly, B.T., Jennings, A.E., Stoner, J.S., Nielsen, T., Andresen, K.J., Nørmark, E., Heirman, K.A., Kamla, E., Jerram, K., Stranne, C., Mix, A., 2020. Glacial sedimentation, fluxes and erosion rates associated with ice retreat in Petermann Fjord and Nares Strait, north-west Greenland. *Cryosphere* 14, 261–286. <https://doi.org/10.5194/tc-14-261-2020>.
- Howe, J.A., Austin, W.E.N., Forwick, M., Paetzl, M., Harland, R., Cage, A.G., 2010. Fjord systems and archives: a review. *Geol. Soc. Spec. Publ.* 344, 5–15. <https://doi.org/10.1144/SP344.2>.
- Hubberten, H.-W., 1995. The expedition ARKTIS-X/2 of RV “polarstern”. In: 1994., *Berichte zur Polarforschung*. Alfred Wegener Institut, Bremerhaven.

- Hughes, A.L.C., Rainsley, E., Murray, T., Fogwill, C.J., Schnabel, C., Xu, S., 2012. Rapid response of Helheim Glacier, southeast Greenland, to early Holocene climate warming. *Geology* 40, 427–430. <https://doi.org/10.1130/G32730.1>.
- Jakobsson, M., Hogan, K.A., Mayer, L.A., Mix, A., Jennings, A., Stoner, J., Eriksson, B., Jerram, K., Mohammad, R., Pearce, C., Reilly, B., Stranne, C., 2018. The Holocene retreat dynamics and stability of Petermann Glacier in northwest Greenland. *Nat. Commun.* 9. <https://doi.org/10.1038/s41467-018-04573-2>.
- Jakobsson, M., Mayer, L.A., Bringenspar, C., Castro, C.F., Mohammad, R., Johnson, P., Ketter, T., Accettella, D., Amblas, D., An, L., Arndt, J.E., Canals, M., Casamor, J.L., Chauché, N., Coakley, B., Danielson, S., Demarte, M., Dickson, M.L., Dorschel, B., Dowdeswell, J.A., Dreutter, S., Fremand, A.C., Gallant, D., Hall, J.K., Hehemann, L., Hodnesdal, H., Hong, J., Ivaldi, R., Kane, E., Klaucke, I., Krawczyk, D.W., Kristoffersen, Y., Kuipers, B.R., Millan, R., Masetti, G., Morlighem, M., Noormets, R., Prescott, M.M., Reberasco, M., Rignot, E., Semiletov, I., Tate, A.J., Travaglini, P., Velicogna, I., Weatherall, P., Weinreb, W., Willis, J.K., Wood, M., Zarayskaya, Y., Zhang, T., Zimmermann, M., Zinglersen, K.B., 2020. The international bathymetric Chart of the arctic ocean version 4.0. *Sci. Data* 7. <https://doi.org/10.1038/s41597-020-0520-9>.
- Jennings, A.E., Weiner, N.J., 1996. Environmental change in eastern Greenland during the last 1300 years : evidence from foraminifera and lithofacies in Nansen Fjord, 68°N. *Holocene* 6, 179–191.
- Johnsen, S.J., Clausen, H.B., Dansgaard, W., Gundestrup, N., Hansson, M., Jonsson, P., Steffensen, J.P., Sveinbjörnsdóttir, A.E., 1992. A “deep” ice core from East Greenland. *Meddelelser om Grønland* 30, 22.
- Koç, N., Jansen, E., Hafflidason, H., 1993. Paleocceanographic reconstructions of surface ocean conditions in the Greenland, Iceland and Norwegian Seas through the last 14 ka based on diatoms. *Quat. Sci. Rev.* 12, 115–140.
- Kolling, H.M., Stein, R., Fahl, K., Perner, K., Moros, M., 2017. Short-term variability in late Holocene sea ice cover on the East Greenland Shelf and its driving mechanisms. *Palaeogeogr. Palaeoclimatol.* 485, 336–350. <https://doi.org/10.1016/j.palaeo.2017.06.024>.
- Kroon, A., Abermann, J., Bendixen, M., Lund, M., Sigsgaard, C., Skov, K., Hansen, B.U., 2017. Deltas, freshwater discharge, and waves along the Young Sound, NE Greenland. *Ambio* 46, 132–145. <https://doi.org/10.1007/s13280-016-0869-3>.
- Laberg, J.S., Forwick, M., Husum, K., 2017. New geophysical evidence for a revised maximum position of part of the NE sector of the Greenland ice sheet during the last glacial maximum. *Arktos* 3, 3. <https://doi.org/10.1007/s41063-017-0029-4>.
- Lambeck, K., Rouby, H., Purcell, A., Sun, Y., Sambridge, M., 2014. Sea level and global ice volumes from the Last Glacial Maximum to the Holocene. *P. Natl. Acad. Sci. USA* 111, 15296–15303. <https://doi.org/10.1073/pnas.1411762111>.
- Larsen, P.-H., Olsen, H., Clack, J.A., 2008. The Devonian basin in East Greenland—A review of basin evolution and vertebrate assemblages. In: Higgins, A.K., Gilotti, J. Smith, M.P. (Eds.), *The Greenland Caledonides. Evolution of the Northeast Margin of Laurentia. Geological Society of America*, pp. 273–292.
- Levy, L.B., Kelly, M.A., Lowell, T.V., Hall, B.L., Hempel, L.A., Honsaker, W.M., Lusas, A.R., Howley, J.A., Axford, Y.L., 2014. Holocene fluctuations of Brege ice cap, Scoresby Sund, east Greenland: a proxy for climate along the Greenland Ice Sheet margin. *Quat. Sci. Rev.* 92, 357–368. <https://doi.org/10.1016/j.quascirev.2013.06.024>.
- Lindeman, M.R., Straneo, F., Wilson, N.J., Toole, J.M., Krishfield, R.A., Beird, N.L., Kanzow, T., Schaffer, J., 2020. Ocean circulation and variability beneath Nioghalvfjædsbræ (79 North Glacier) ice tongue. *J. Geophys. Res.-Ocean* 125, 1–20. <https://doi.org/10.1029/2020JC016091>.
- Luostarinen, T., Ribeiro, S., Weckström, K., Sejr, M., Meire, L., Tallberg, P., Heikkilä, M., 2020. An annual cycle of diatom succession in two contrasting Greenlandic fjords: from simple sea-ice indicators to varied seasonal strategists. *Mar. Micropaleontol.* 158. <https://doi.org/10.1016/j.marmicro.2020.101873>.
- Mankoff, K.D., Colgan, W., Solgaard, A., Karlsson, N.B., Ahlström, A.P., Van As, D., Box, J.E., Abbas Khan, S., Kjeldsen, K.K., Mougintot, J., Fausto, R.S., 2019. Greenland Ice Sheet solid ice discharge from 1986 through 2017. *Earth Syst. Sci. Data* 11, 769–786. <https://doi.org/10.5194/essd-11-769-2019>.
- Mariénfeld, P., 1992. Postglacial sedimentary history of Scoresby Sund, east Greenland. *Polarforschung* 60, 181–195.
- Mitchum, R.M.J., Vail, P.R., Sangree, J.B., 1977. Seismic stratigraphy and global changes of sea level, Part 6 : stratigraphic interpretation of seismic reflection patterns in depositional sequences. In: Payton, C. (Ed.), *Seismic Stratigraphy - Applications to Hydrocarbon Exploration. The American Association of Petroleum Geologists, Tulsa, Oklahoma, USA*, pp. 117–134.
- Müller, J., Werner, K., Stein, R., Fahl, K., Moros, M., Jansen, E., 2012. Holocene cooling culminates in sea ice oscillations in Fram Strait. *Quat. Sci. Rev.* 47, 1–14. <https://doi.org/10.1016/j.quascirev.2012.04.024>.
- Munsell, A.H., 2000. *Munsell Soil Color Charts*. Munsell Color Company. <https://doi.org/10.1111/1911-3846.12037>.
- Muntjewerf, L., Pettrini, M., Vizcaino, M., Ermani da Silva, C., Sellevold, R., Scherrenberg, M.D.W., Thayer-Calder, K., Bradley, S.L., Lenaerts, J.T.M., Lipscomb, W.H., Lofverstrom, M., 2020. Greenland Ice Sheet contribution to 21st century sea level rise as simulated by the coupled CESM2.1-CISM2.1. *Geophys. Res. Lett.* 47. <https://doi.org/10.1029/2019GL086836>.
- Newton, A.M.W., Knutz, P.C., Huuse, M., Gannon, P., Brocklehurst, S.H., Clausen, O.R., Gong, Y., 2017. Ice stream reorganization and glacial retreat on the northwest Greenland shelf. *Geophys. Res. Lett.* 44, 7826–7835. <https://doi.org/10.1002/2017GL073690>.
- Noël, B., van de Berg, W.J., Lhermitte, S., van den Broeke, M.R., 2019. Rapid ablation zone expansion amplifies north Greenland mass loss. *Sci. Adv.* 5. <https://doi.org/10.1126/sciadv.aaw0123>.
- Ó Cofaigh, C., Dowdeswell, J.A., 2001. Laminated sediments in glacial marine environments: diagnostic criteria for their interpretation. *Quat. Sci. Rev.* 20, 1411–1436. [https://doi.org/10.1016/S0277-3791\(00\)00177-3](https://doi.org/10.1016/S0277-3791(00)00177-3).
- Ó Cofaigh, C., Dowdeswell, J.A., Evans, J., Kenyon, N.H., Taylor, J., Mienert, J., Wilken, M., 2004. Timing and significance of glacially influenced mass-wasting in the submarine channels of the Greenland Basin. *Mar. Geol.* 207, 39–54. <https://doi.org/10.1016/j.margeo.2004.02.009>.
- Ó Cofaigh, C., Dowdeswell, J.A., Grobe, H., 2001. Holocene glacial marine sedimentation, inner Scoresby Sund, East Greenland: the influence of fast-flowing ice-sheet outlet glaciers. *Mar. Geol.* 175, 103–129. [https://doi.org/10.1016/S0025-3227\(01\)00117-7](https://doi.org/10.1016/S0025-3227(01)00117-7).
- Ó Cofaigh, C., Dowdeswell, J.A., Jennings, A.E., Hogan, K.A., Kilfeather, A., Hiemstra, J.F., Noormets, R., Evans, J., McCarthy, D.J., Andrews, J.T., Lloyd, J.M., Moros, M., 2013. An extensive and dynamic ice sheet on the west Greenland shelf during the last glacial cycle. *Geology* 41, 219–222. <https://doi.org/10.1130/G33759.1>.
- Olsen, I.L., Rydningen, T.A., Forwick, M., Laberg, J.S., Husum, K., 2020. Last glacial ice sheet dynamics offshore NE Greenland – a case study from Store Koldewey Trough. *Cryosphere* 14, 4475–4494. <https://doi.org/10.5194/tc-14-4475-2020>.
- Plassen, L., Vorren, T.O., Forwick, M., 2004. Integrated acoustic and coring investigation of glacialic deposits in Spitsbergen fjords. *Polar Res.* 23, 89–110. <https://doi.org/10.1111/j.1751-8369.2004.tb00132.x>.
- Pritchard, H.D., Arthern, R.J., Vaughan, D.G., Edwards, L.A., 2009. Extensive dynamic thinning on the margins of the Greenland and Antarctic ice sheets. *Nature* 461, 971–975. <https://doi.org/10.1038/nature08471>.
- Prothro, L.O., Simkins, L.M., Majewski, W., Anderson, J.B., 2018. Glacial retreat patterns and processes determined from integrated sedimentology and geomorphology records. *Mar. Geol.* 395, 104–119. <https://doi.org/10.1016/j.margeo.2017.09.012>.
- Rasmussen, S.O., Vinther, B.M., Clausen, H.B., Andersen, K.K., 2007. Early Holocene climate oscillations recorded in three Greenland ice cores. *Quat. Sci. Rev.* 26, 1907–1914. <https://doi.org/10.1016/j.quascirev.2007.06.015>.
- Reimer, Paula J., Austin, W.E.N., Bard, E., Bayliss, A., Blackwell, P.G., Bronk, C., Butzin, M., Cheng, H., Edwards, R.L., Friedrich, M., Grootes, P.M., Guilderson, T.P., Hajdas, I., Heaton, T.J., Hogg, A.G., Hughen, K.A., Kromer, B., Manning, S.W., Muscheler, R., Palmer, J.G., Pearson, C., Plicht, J. Van Der, Reimer, R.W., Richards, D.A., Scott, E.M., Southon, J.R., Turney, C.S.M., Wacker, L., Adolphi, F., Reimer, P.J., 2020. The IntCal Northern Hemisphere radiocarbon age calibration curve (0–55 cal kBP). *Radiocarbon* 62, 725–757. <https://doi.org/10.1017/RDC.2020.41>.
- Ribeiro, S., Sejr, M.K., Limoges, A., Heikkilä, M., Andersen, T.J., Tallberg, P., Weckström, K., Husum, K., Forwick, M., Dalsgaard, T., Massé, G., Seidenkrantz, M.S., Rysgaard, S., 2017. Sea ice and primary production proxies in surface sediments from a High Arctic Greenland fjord: spatial distribution and implications for palaeoenvironmental studies. *Ambio* 46, 106–118. <https://doi.org/10.1007/s13280-016-0894-2>.
- Saheer, M., Klitgaard, D., Hald, M., Pavlova, O., Lindal, L., 2012. Changes in distribution of calcareous benthic foraminifera in the central Barents Sea between the periods 1965 – 1992 and 2005 – 2006. *Glob. Planet. Change* 98–99, 81–96. <https://doi.org/10.1016/j.gloplacha.2012.08.006>.
- Seale, A., Christoffersen, P., Mugford, R.I., O’Leary, M., 2011. Ocean forcing of the Greenland Ice Sheet: calving fronts and patterns of retreat identified by automatic satellite monitoring of eastern outlet glaciers. *J. Geophys. Res.-Earth* 116, 1–16. <https://doi.org/10.1029/2010JF001847>.
- Smith, L.M., Andrews, J.T., 2000. Sediment characteristics in iceberg dominated fjords, Kangerlussuaq region, East Greenland. *Sediment. Geol.* 130, 11–25. [https://doi.org/10.1016/S0037-0738\(99\)00088-3](https://doi.org/10.1016/S0037-0738(99)00088-3).
- Stein, R., Nam, S.-I., Grobe, H., Hubberten, H.-W., 1996. Late Quaternary glacial history and short-term ice-raftered debris fluctuations along the East Greenland continental margin. In: Andrews, J.T., Austin, W.E.N., Bergsten, H., Jennings, A.E. (Eds.), *Late Quaternary Palaeoceanography of the North Atlantic Margins. Geological Society of London, Special Publications*, pp. 135–151.
- Streuff, K., Ó Cofaigh, C., Hogan, K., Jennings, A., Lloyd, J.M., Noormets, R., Nielsen, T., Kuipers, A., Dowdeswell, J.A., Weinreb, W., 2017. Seafloor geomorphology and glacial marine sedimentation associated with fast-flowing ice sheet outlet glaciers in Disko Bay, West Greenland. *Quat. Sci. Rev.* 169, 206–230. <https://doi.org/10.1016/j.quascirev.2017.05.021>.
- Stuiver, M., Reimer, P.J., Reimer, R.W., 2020. CALIB 8.2 [WWW program] [WWW Document]. URL <http://calib.org>, 10.13.20.
- Syvitski, J.P.M., 2003. Sediment fluxes and rates of sedimentation. In: Middleton, G.V., Church, M.J., Coniglio, M., Hardie, L.A., Longstaffe, F.J. (Eds.), *Encyclopedia of Sediments and Sedimentary Rocks*. Springer Netherlands, Dordrecht, pp. 600–606. https://doi.org/10.1007/978-1-4020-3609-5_180.
- Vasskog, K., Langebroek, P.M., Andrews, J.T., Even, J., Nilsen, O., Nesje, A., 2015. The Greenland Ice Sheet during the last glacial cycle : current ice loss and contribution to sea-level rise from a palaeoclimatic perspective. *Earth Sci. Rev.* 150, 45–67. <https://doi.org/10.1016/j.earscirev.2015.07.006>.
- Vermassen, F., Bjørk, A.A., Sicre, M.A., Jaeger, J.M., Wangner, D.J., Kjeldsen, K.K., Siggaard-Andersen, M.L., Klein, V., Mougintot, J., Kjær, K.H., Andresen, C.S., 2020. A major collapse of Kangerlussuaq Glacier’s ice tongue between 1932 and 1933 in East Greenland. *Geophys. Res. Lett.* 47, 1–9. <https://doi.org/10.1029/2019GL085954>.
- Vorren, O., Tore, Plassen, Liv, 2002. Deglaciation and palaeoclimate of the Andfjord-Vågsfjord area, North Norway. *Boreas* 31, 97–125.

- Wagner, B., Bennike, O., Cremer, H., Klug, M., 2010. Late quaternary history of the Kap Mackenzie area, northeast Greenland. *Boreas* 39, 492–504. <https://doi.org/10.1111/j.1502-3885.2010.00148.x>.
- Wagner, B., Melles, M., 2002. Holocene environmental history of western Ymer Ø, East Greenland, inferred from lake sediments. *Quat. Int.* 89, 165–176. [https://doi.org/10.1016/S1040-6182\(01\)00087-8](https://doi.org/10.1016/S1040-6182(01)00087-8).
- Wagner, B., Melles, M., Hahne, J., Niessen, F., Hubberten, H.W., 2000. Holocene climate history of Geographical Society Ø, east Greenland - evidence from lake sediments. *Palaeogeogr. Palaeoclimatol.* 160, 45–68. [https://doi.org/10.1016/S0031-0182\(00\)00046-8](https://doi.org/10.1016/S0031-0182(00)00046-8).
- Walker, M., Head, M.J., Berkelhammer, M., Björck, S., Cheng, H., Cwynar, L., Fisher, D., Gkinis, V., Long, A., Lowe, J., Newnham, R., Rasmussen, S.O., Weiss, H., 2018. Formal ratification of the subdivision of the Holocene series/epoch (Quaternary system/period): two new global boundary stratotype sections and points (GSSPs) and three new stages/subseries. *Episodes* 41, 213–223. <https://doi.org/10.18814/epiiugs/2018/018016>.
- Weidick, A., 1976. C14 dating of survey material carried out in 1975. *Grøn. Geol. Unders.* 80, 136–144.
- Weidick, A., 1977. 14C dating of survey material carried out in 1976. *Grøn. Geol. Unders.* 85, 127–129.
- Winkelmann, D., Jokat, W., Jensen, L., Schenke, H.W., 2010. Submarine end moraines on the continental shelf off NE Greenland - implications for Lateglacial dynamics. *Quat. Sci. Rev.* 29, 1069–1077. <https://doi.org/10.1016/j.quascirev.2010.02.002>.